MOLECULAR DYNAMICS STUDY OF RANDOM AND ORDERED METALS
AND METAL ALLOYS

A THESIS SUBMITTED TO
THE GRADUATE SCHOOL OF NATURAL AND APPLIED SCIENCES
OF
MIDDLE EAST TECHNICAL UNIVERSITY

BY

HASAN HÜSEYİN KART

IN PARTIAL FULFILLMENT OF THE REQUIREMENTS

FOR

THE DEGREE OF DOCTOR OF PHILOSOPHY

IN

PHYSICS

AUGUST 2004

Approval of the Graduate School of Natural and Applied Sciences.

—————————————————
Prof. Dr. Canan Özgen
Director

I certify that this thesis satisfies all the requirements as a thesis for the degree of Doctor of Philosophy.

—————————————————
Prof. Dr. Sinan Bilikmen
Head of Department

This is to certify that we have read this thesis and that in our opinion it is fully adequate, in scope and quality, as a thesis for the degree of Doctor of Philosophy.

—————————————————
Prof. Dr. Mehmet Tomak
Supervisor

Examining Committee Members

Prof. Dr. Bülent Karasözen (METU, MATH)   —————————————

Prof. Dr. Mehmet Tomak (METU, PHYS)   —————————————

Prof. Dr. Mesude Sağlam (Ankara Univ., PHYS) —————————————

Assoc. Prof. Dr. Hatice Kökten (METU, PHYS) —————————————

Assist. Prof. Dr. Sadi Turgut (METU, PHYS)   —————————————

"I hereby declare that all information in this document has been obtained and presented in accordance with academic rules and ethical conduct. I also declare that, as required by these rules and conduct, I have fully cited and referenced all material and results that are not original to this work."

Name Surname : HASAN HÜSEYİN KART

Signature :

ABSTRACT

MOLECULAR DYNAMICS STUDY OF RANDOM AND ORDERED
METALS AND METAL ALLOYS

Kart, Hasan Hüseyin

Ph.D., Department of Physics

Supervisor: Prof. Dr. Mehmet Tomak

August 2004, 106 pages.

The solid, liquid, and solidification properties of Pd, Ag pure metals and especially Pd_xAg_{1-x} alloys are studied by using the molecular dynamics simulation. The effects of temperature and concentration on the physical properties of Pd_xAg_{1-x} are analyzed. Sutton-Chen (SC) and Quantum Sutton-Chen (Q-SC) many-body potentials are used as interatomic interactions which enable one to investigate the thermodynamic, static, and dynamical properties of transition metals. The simulation results such as cohesive energy, density, elastic constants, bulk modulus, pair distribution functions, melting points and phonon dispersion curves obtained for Pd, Ag and Pd_xAg_{1-x} are in good agreement with the available experimental data at various temperatures. The predicted melting points of Pd, Ag and their binary alloys by using Q-SC potential parameters are closer to experimental values than the ones predicted from SC potential parameters.

The liquid properties such as diffusion constants and viscosities computed from Q-SC potentials are also in good agreement with the available experimental data and theoretical calculations. Diffusion coefficients and viscosity results calculated from simulation obey the Arrhenius equation well. The coefficients of the Arrhenius equation are given in order to calculate the self-diffusion coefficient and shear viscosity of Pd-Ag alloys at the desired temperature and concentration.

Using different cooling rates, we investigate glass formation tendency and crystallization of Pd-Ag metal alloys, by analyzing pair distribution function, enthalpy, volume, and diffusion coefficient. Pd-Ag alloys show the glass structure at fast cooling rates while it crystallizes at slow cooling rates. Glass and crystallization temperatures are also obtained from the Wendt-Abraham parameter. The split of the second peak in the pair distribution function is associated with the glass transition. Glass forming ability increases with increasing concentration of Ag in Pd-Ag alloys.

Thermal and mechanical properties of Cu, Au metals and their ordered intermetallic alloys $Cu_3Au(L1_2)$, $CuAu(L1_0)$, and $CuAu_3(L1_2)$ are also studied to investigate the effects of temperature and concentration on the physical properties of Cu-Au alloys. The simulation results such as cohesive energy, lattice parameter, density, elastic constants, bulk modulus, heat capacity, thermal expansion, melting points, and phonon dispersion curves are in good agreement with the available experimental and theoretical data at various temperatures.

The Q-SC potential parameters are more reliable in determining physical properties of metals and their random and ordered alloys studied in this work.

Keywords: Molecular Dynamics, Metals and Metal Alloys, Pd-Ag, Cu-Au, Intermetallic Alloys, Thermal and Mechanical Properties, Phonon Dispersion Relations, Liquid Metals, Metallic Glasses, Diffusion Coefficient, Viscosity, Heat Capacity, Thermal Expansion.

ÖZ

DÜZENLİ VE DÜZENSİZ METAL VE METAL ALAŞIMLARININ
MOLEKÜLER-DİNAMİK ÇALIŞMASI

Kart, Hasan Hüseyin

Doktora, Fizik Bölümü

Tez Yöneticisi: Prof. Dr. Mehmet Tomak

Ağustos 2004, 106 sayfa.

Pd, Ag metallerinin ve Pd-Ag alaşımlarının katı, sıvı ve soğutma özellikleri moleküler dinamik simülasyonu ile çalışıldı. Sıcaklığın ve konsantrasyonun Pd-Ag alaşımının fiziksel özelliklerine olan etkisi araştırıldı. Geçiş metalleri ve metal alaşımlarının termodinamik, statik, ve dinamik özelliklerini araştırmak için, atomlar arası etkileşmeleri tanımlayan Sutton-Chen (SC) ve quantum Sutton-Chen (Q-SC) çok cisimli potensiyelleri kullanıldı. Pd, Ag ve Pd-Ag alaşımlarının bağlanma enerjisi, yoğunluk, elastik sabiti, bulk modülüs, çift dağılım fonksiyonu, erime sıcaklığı ve fonon dispersiyon ilişkilerinin değişik sıcaklıklardaki deneysel değerlerle uyum içinde olduğu gözlendi. Q-SC potansiyel parametreleri ile hesaplanan erime noktaları SC potansiyeli ile hesaplanan değerlere göre deneysel değerlere daha yakındır.

Difüzyon, viskosite gibi Q-SC potansiyeli ile hesaplanan sıvı özellikler deneysel ve teorik değerlerle uyum içindedir. Simülasyondan hesaplanan difüzyon katsayısı ve viskosite Arrhenius denklemine iyi bir şekilde uymaktadır. Arrhenius denkleminin katsayıları, farklı sıcaklık ve karışımlarda diffüzyon ve viskositeyi hesaplamak için elde edildi.

Farklı soğutma oranları kullanılarak, Pd-Ag alaşımının kristalleşme ve camsı yapı göstermesi, çift dağılım fonksiyonu, entalpi, hacim ve difüzyon katsayısı

vi

analiz edilerek incelenmiştir. Camsı yapı ve kristalleşme sıcaklıkları Wendt-Abraham parametresi kullanılarak da elde edilmiştir. Çift dağılım fonksiyonundaki ikinci tepenin yarılması camsı yapının bir özelliği olarak düşünülür.

Bu çalışmada ayrıca bakır (Cu) ve altın (Au) metallerinin ve bu metallerin oluşturduğu $Cu_3Au(L1_2)$, $CuAu(L1_0)$, ve $CuAu_3(L1_2)$ düzenli bakır ve altın alaşımlarının sıcaklığa bağlı fiziksel özellikleri araştırıldı. Elde edilen bağlanma enerjisi, örgü sabiti, yoğunluk, elastik sabiti, bulk modülüs, ısı sığası, ısısal genleşme, erime noktası, ve fonon dispersiyon ilişkisi gibi özelliklerin deneysel ve diğer çalışmalarla uyumlu olduğu gözlendi.

Q-SC potansiyel parametreleri bu çalışmada incelenen metal ve metal alaşımlarının fiziksel özelliklerinin belirlenmesinde daha güvenilir olduğu tesbit edildi.

Anahtar Kelimeler: Moleküler Dinamik, Metaller ve Metal Alaşımları, Pd-Ag, İntermetaller, Cu-Au, Termal ve Mekanik Özellikler, Phonon Dispersiyon İlişkisi, Sıvı Metaller, Metalik Camlar, Diffüzyon Katsayısı, Viskosite, Isı Sığası, Isısal genişleme.

... MY WIFE

and

... MY DAUGHTER

ACKNOWLEDGMENTS

I would like to thank my supervisor Prof. Dr. Mehmet Tomak for his support, encouragement, and guidance, for the trust and freedom he gave me during my graduate work and for enlightening my life and career.

I also want to thank Dr. Tahir Çağın for providing molecular dynamics simulation program and for discussion about our simulation results.

My special thanks go to Dr. Mustafa Uludoğan for making me be familiar with the simulation program and for solving the technical problems.

My special thanks also go to Assoc. Prof. Hatice Kökten for helping overcome the struggling time and for advice on science and life. I would like to thank Sema Memiş and Dr. Ali Çoruh for friendships. Special thanks to all staffs of department of physics at METU for their encouragement and friendship.

I would like to thank Dr. Sadi Turgut for editing this thesis.

Finally, I dedicate this thesis to my wife and my daughter. I would like to express my gratitude and my appreciation to my wife for her love, moral support and encouragement, helping me write this thesis, and giving me a happy and complete life. I am very much indebted to my family for their support and their love.

TABLE OF CONTENTS

LIST OF TABLES

LIST OF FIGURES

CHAPTER 1

INTRODUCTION

Computational modeling of material behavior and material design are becoming reliable tools for scientific investigations and they complement traditional theoretical and experimental approaches. The system-driven computational design approaches save the cost of discovery, by using computers to design, characterize, and optimize materials before beginning the expensive experimental processes of characterization, synthesis, processing and testing [1, 2, 3, 4, 5, 6, 7]. The different physical theories such as quantum mechanics, molecular dynamics, and statistical mechanics are incorporated properly on various length and time scales to design new alloys or pure materials.

Most of the phenomena in the low-energy physics, chemistry, materials science and biology can be explained by quantum mechanical description of the electrons and the ions. The properties and the behavior of materials are derived from the quantum mechanical description of events at the atomistic scale in many cases. The ability of quantum mechanics to predict total energy and atomic structure of a system of electrons and nuclei enables one to obtain an enormous benefit from a quantum mechanical calculation. Many methods such as pseudopotentials [8] and density functional theory [7] have been developed for solving the Schrödinger

equation that can be used to calculate the total energies of assemblies of atoms and forces between the atoms. Another very significant theoretical milestone was the 1985 paper of Car and Parrinello [9], which showed the way to calculate the total energies and forces on atoms. The number of atoms which can be simulated by *ab initio* techniques has grown since the Car-Parrinello paper. These methods are still based on pseudopotential and density functional theory. The system of atoms simulated from *ab initio* method means simulation without introducing any fitting parameters [7].

The application of *ab initio* methods to real materials is still limited. At the moment even if the fastest supercomputers with the largest memory are employed, a few hundred atoms can be treated with a simulation time of a few picoseconds. Such methods serve two important purposes. Firstly, they provide direct information on the response of materials to external environments. Secondly, they also produce a database of properties that can be used to construct effective (empirical) interatomic potentials. Thus, the next step of coarse graining the problem is to remove the electronic degrees of freedom by imagining the atoms to be held together by some sort of glue or interatomic potentials, allowing one large-scale atomistic simulation for millions of atoms and a simulation time of nanoseconds.

Atomistic simulations by using interatomic potentials [3, 10, 11] are extremely useful in investigating the properties of a physical system. Interatomic potentials involve fitting the parameters to a predetermined experimental or *ab initio*

database, which includes physical quantities such as lattice constants, elastic constants, vacancy formation energy and surface energy.

The atomic interaction must be approximated to determine the properties of an ensemble of atoms larger than that handled by computational quantum mechanics. The molecular dynamics (MD) method is developed to study the properties of material in volumes containing millions to billions of atoms with effective interatomic potentials. The interaction between two atoms is defined by a potential function that depends on the atomic configurations (i.e. relative displacement) and the local environment (i.e. electrons).

The computations using accurate many-body potentials (empirical or first-principle derived) may be used to simulate metallic systems with many atoms. It is relatively easier to investigate many systems with a classical approach that enables one to determine trends in physical properties. An important development in the classical description of interatomic forces is going beyond the two body description, by introduction of many-body terms akin tight binding scheme, or density dependence as in embedded atom model (EAM). The main advantage of a many-body treatment over the conceptually and practically simpler and successful pair-potential description is the ability to better reproduce some basic features of the transition metals [12, 13, 14, 15]. Some of these approaches are the empirical many-body potentials based on Norskov's effective medium theory [17], Daw and Baskes's embedded atom method [12], Finnis and Sinclair's empirical many-body potentials [13] and more recently the many-body potentials

3

developed by Sutton and Chen [15] within the context of tight binding approach for fcc transition metals.

One of the main problems in the application of inter-atomic potentials is the transferability of parameters. Interatomic potentials are usually fitted to some experimental or first-principle results at solid phase. However, it is not clear whether simulations carried out at elevated temperatures, such as at liquid phase and during the solidification process, still reproduce the experimental data. Comparison of the simulation results and experimental data at various temperatures can thus serve as a measure of the reliability and the utility of a potential model.

Transition metals and their alloys are very important both scientifically and technologically. For example, Pd is used as delicate mainsprings in analog wristwatches, in surgical instruments, as a catalyst, and also used as a substitute for silver in dental items and jewelery. Ag is used in alloys, for jewelery and in other compounds for photography and in conductors. Pd-Ag alloys are also used as catalysts and their surfaces present many interesting technological characteristics. Recently, interest in Pd-Ag alloys has greatly increased with applications in domains such as dentistry, LCD screen, and hydrogen separation and storage [16]. Therefore, understanding of the properties for Pd-Ag system of various concentrations and at various temperatures are important. However, there is not much comprehensive experimental and theoretical studies for the temperature and concentration dependence of various properties of especially metallic alloys at various

temperatures. Recently, Papanicolaou *et al.* [18] studied Cu-Au alloys by evaluating interatomic potentials of Cu, Au, and Cu-Au ordered alloys by fitting potential parameters to the volume dependence of the total energy computed from first-principles augmented-plane-wave (APW) calculations. Papanicolaou and Papaconstantopolos [19] developed a many-body interatomic potential for Pd by using the same procedure with LAPW. Feraoun *et al.* [20] used the modified embedded atom model to study mechanical and thermodynamical properties of Cu-Ag systems at different concentrations with the pure elemental potential parameters. The same authors [21] predicted physical properties of Cu-Ag alloys with Sutton-Chen potential by fitting to the first-principle calculations. Lovvik and Olsen [22] studied bulk properties of pure Pd, Ag, and their binary alloys by using periodic bulk calculations based on density functional theory within the generalized gradient approximation (GGA). Liu *et al.* [23] investigated the thermodynamical and melting points of Ni_3Al and Cu_3Au by using the tight binding potentials. Clearly much more work needs to be done in this area. Some approximations have been made to obtain potential parameters for determining physical properties of alloys. Thus it is of interest to develop potential parameters for binary intermetallic alloy system without changing the available parameter of pure elemental case.

From the experimental and theoretical points of view, metallic liquid alloys appear to be less studied than pure liquids since their description is more difficult.

Recently Wax *et al.* [24] studied structure of liquid alloys of alkali metals by using molecular dynamics. Qi *et al.* [25] predicted viscosity of Au-Cu liquid metal alloys via quantum Sutton-Chen potential by a non-equilibrium molecular dynamics. Asta *et al.* [26] studied structural, thermodynamic, and atomic-transport properties of liquid Ni-Al alloys by embedded-atom model via Monte Carlo and molecular dynamics simulations. Ji and Gong [27] investigated the temperature-dependent properties of Al-Si liquid alloys by using *ab initio* molecular dynamics technique.

The knowledge of the diffusion coefficients in liquid metals is important for a reasonable prediction of mass transfer rates in a number of existing and potential applications including the pro-metallurgical re-processing of spent fuels from nuclear reactors, and in the production of metallic alloys in liquid phases. Several processes such as corrosion, phase separation, crystal growth, etc. are governed by the rates of mass transfer which are primarily dependent on the values of relevant diffusion coefficients [28]. Moreover, many physical properties of material, such as the bond energy and force constants, directly affect the rate at which atoms diffuse. Viscosity is also very important for understanding the dynamics of liquids. Experimental data for self-diffusivities and viscosities of liquid metals and metallic alloys are scarce except for some metals at some specific temperatures. So it is interesting to simulate liquid transition metals and their binary alloys, and to calculate the transport properties using computer simulations. The casting engineer relies also on either theoretical or phenomenological models for

6

their values.

Metallic glasses, i.e, the amorphous solid phases formed by ultra-rapid cooling of liquid alloys, are also fascinating materials because of their unique physical properties. A complete and satisfactory theory of the microscopic properties of a metallic liquid at low temperatures is still an unsolved problem. Supercooled liquids at temperatures below their melting point, which have avoided crystallization, can be cooled below the glass transition temperature to form a glass or an amorphous solid. The understanding of the structure and thermal stability of these metastable materials is of great importance from both the fundamental and practical points of view [29, 30]. They challenge one to describe the structure and atomic dynamics of a system out of equilibrium [31, 32]. Their stability and formation have been correlated with electronic effects [33], metal-alloy chemistry and eutectic composition [34]. They are extremely ductile and resistant to corrosion and there are many applications in the industry [35, 36, 37]. Much research has been devoted to the study of bulk metallic glasses [34, 38, 39, 40, 41, 42, 43, 44, 45, 46, 47] since the discovery in 1960 by Duwez and co-workers [48].

Alloys based on the ordered intermetallic compounds constitute a unique class of metallic materials that form a crystal structure. These alloys are strong, stiff, and ductile at high temperatures. They have structure and properties that differ greatly from constituent metals, but alloys are solid solutions between different metals. Many intermetallic compounds display an attractive combination of

physical and mechanical properties including high melting point, low density and good oxidation or corrosion resistance. They are also typically brittle, highly crystalline compounds that form in given proportions. These kind of properties have motivated the strong interest in understanding their fundamental properties [49, 50, 51, 52, 53, 54].

Cu-Au is especially a well-known model for binary intermetallic systems, it is well-known due to the existence of a temperature-induced order-disorder transition and capability of the stable long period superlattice structure. Cu_3Au, CuAu and $CuAu_3$ intermetallic alloys are of potential use in industry because of the properties mentioned above. A lot of experimental and theoretical research has been focused on these alloy systems both experimentally and theoretically [55, 56, 57, 58, 59, 60, 61, 62, 63, 64, 65, 66, 67, 68, 69, 70, 71, 72] but relatively little attention has been paid to the temperature dependence of the thermodynamical and mechanical properties of the ordered Cu-Au intermetallic compounds. The experimental studies of their properties are still a very difficult problem because of their high melting points. Now, we have sparse experimental values related to the these materials in literature. This affects the progress in developing novel intermetallic compounds and alloys.

The molecular dynamics (MD) method [73] is currently one of the most powerful tools for obtaining the macroscopic and microscopic features of the materials and has been used to investigate solid, liquid, glass formation and crystallization processes of materials by using different types of interatomic potentials. In an

MD simulation, the motion of individual atoms within an assembly of N atoms or molecules is modeled on the basis of Newtonian dynamics, given the initial positions and velocities of the atoms. A finite model consisting of N atoms confined in a simulation cell of volume V is initially constructed in any classical simulation. The cell is replicated in all spatial dimensions generating its own periodic images as well as those of the original N atoms. The imposition of periodic boundary condition (PBC) is necessary so as to compensate for undesirable effects of the artificial surfaces associated with the finite size of the simulated system. The energetics and dynamics of the atoms are obtained from prescribed phenomenological inter-atomic potentials. MD can provide important insight by allowing one to determine quantities which are difficult to access in real experiments and hard to obtain with reasonable precision.

Sutton-Chen (SC) [15] and quantum Sutton-Chen (Q-SC) [74] many-body potentials are used in this study. Their binary alloy parameters are derived from pure elemental parameters as given in the following chapter.

The purpose of the present work is to perform a comprehensive study of the solid state, melting behavior, liquid state, and solidification properties of Pd, Ag pure metals and Pd_xAg_{1-x} alloys. We intend to show the validity of SC and Q-SC potential energy functions for these materials at elevated temperatures. We are particularly interested in testing the transferability of the potential from pure elemental form to the alloy case and from solid to liquid phase without further empirical fitting to properties of Pd-Ag alloys and in investigating the

9

performance of SC and Q-SC potentials on different state properties. The transferability is checked by using dynamical properties as well as structural properties of Pd-Ag liquid alloys. The results for solid and liquid states obtained by using Q-SC potential are also compared with SC and other potential calculations. In this study, we have tried to cover most of the static and dynamical properties of the Pd-Ag system not available in the literature. This study also presents the solid and melting behavior properties of both Cu, Au pure metals and ordered intermetallic alloys of Cu_3Au, CuAu, $CuAu_3$.

The outline of this thesis is as follows: Chapter 2 describes the MD method and gives the main simulation procedure for carrying out the calculations in different ensembles to find various properties of a physical system. The pertinent interatomic potentials for the elemental and binary alloy systems, especially Sutton-Chen potentials and some formalism are given in Chapter 3 to provide some necessary theoretical expression required in this study. The results for solid, liquid, and solidification properties of Pd-Ag system are given and discussed in Chapter 4. Section 4.1 is concerned with the solid and melting properties of the metals. A comprehensive liquid property of the system is reported in Section 4.2. This is then followed by the calculation of the glass formation and crystallization properties of the metallic Pd-Ag system in Section 4.3. Section 4.4 deals with the studies of intermetallic alloys of Cu_3Au, CuAu, $CuAu_3$ and Cu, Au pure metals. Finally, the conclusions are presented in Chapter 5.

CHAPTER 2

MOLECULAR DYNAMICS

2.1 Molecular Dynamics Simulation

Statistical mechanics provides a means for determining physical properties of a macroscopic sample of a bulk solid, liquid, and so on. This is done by finding the properties of many atoms or molecules in many possible energy states. The difficult part of this process is to find the information about all possible energy states. One way for obtaining the information about the system is to use molecular dynamics (MD) simulation [73, 75, 76, 77].

Molecular dynamics method is a simulation of the time dependent behavior of atoms or molecules that make up a system, and it is essentially deterministic in nature. MD simulations allow us to calculate the static properties as well as dynamical properties of the system.

In general, steps followed in this technique are given as [78];

1- Choose initial positions for the atoms.

2- Choose initial set of atomic velocities.

3- Compute the momentum of each atom from its velocity and mass.

4- Compute the forces on each atom from an energy expression which is detailed in the Chapter 3.

5- Compute new positions for the atoms a short time later. This is a numerical integration of Newton's equation of motion by using the previous information of the atoms.

6- Compute new velocity and accelerations of the atoms.

7- Repeat steps 3-6.

8- Repeat this iteration long enough for the system to reach equilibrium.

9- After reaching the equilibrium state, begin saving the atomic coordinates, velocities, and accelerations at every few steps.

10- Go on iterating and saving data until the necessary data have been collected to calculate the macroscopic physical quantities with the desired accuracy.

11- Finally, analyze the trajectory to obtain the information about the system by taking as time average over the dynamical history of the system.

These steps may be summarized in the three categories; initialization, equilibration and production. Initialization establishes the thermodynamic state and assigns initial positions and velocities to the atoms. Equilibration develops the dynamics over a sufficient time for the system to forget how it was prepared. Simulation generates the equilibrium phase-space trajectory from which properties will be calculated after the equilibration of the system.

2.2 Innovations in Molecular Dynamics

Molecular dynamics method for study of condensed phases was first carried out by Alder and Wainwright [79, 80]. Then, Rahman [81, 82, 83] used this method

to extend the case where the particles of the fluid interact through continuous potentials which is called Lennard-Jones potential. A more systematic study of the properties of the Lennard-Jones fluid was made by Verlet and co-workers [84, 85, 86, 87]. Since then, this popular method has been applied to a wide range of increasingly complex systems, including liquid metals, molten salts, and molecular liquids of many types.

There are several ensembles, called EVN, HPN, TPN, TVN, μTV, and μTP, where N, E, V, T, P, H and μ denote, respectively, the number of particles, total energy, the volume, the temperature, pressure, the enthalpy and the chemical potential in statistical thermodynamics. For example, the EVN ensemble is the so-called microcanonical ensemble, where the quantities E, V and N are held constant. (In the microcanonical ensemble the basic equation of motion is the Newtonian equation, but in other ensembles this is not necessarily the case). The TVN ensemble is the canonical ensemble, where T, V and N are held constant [7]. The other ensembles are named similarly. The basic equations for the evaluation of the particle positions are chosen according to the different ensembles one wishes to simulate.

The MD method were limited to the study of the system with the specified values of N, V, and E until 1980's. It is desirable to perform simulation at constant temperature and/or pressure, under conditions in which the energy and volume of the system can fluctuate in some situations. Several schemes have

been developed for this purpose, most of them are inspired by a paper of Andersen [88]. They are based on a reformulation of the Lagrangian equation of motion of the system. The works of Andersen and later that of Nosé [89, 90] are based on the concept of an "extended" system consisting of the physical system and an external reservoir. The coupling to the reservoir serves to maintain constancy of pressure or temperature (or both) by a suitable modification of the equation of motion of the particles in the system. The system proposed by Andersen [88], consisting of N particles with coordinates r_i, is assumed to be coupled to an external piston. The reason for using piston in this system is to contract or expand the system uniformly in response to any imbalance between the instantaneous pressure within the system and the externally set pressure. This extended system may be described by a fluctuating volume V and scaled coordinates $\tau_i = V^{-1/3} r_i$ for r_i in the box of volume V, each component of τ_i is a dimensionless number between zero and one. Andersen has shown that how MD calculation can be modified to study under constant pressure by introducing the volume of the system as an additional dynamical variable. Parrinello and Rahman extended the method to allow for changes of the molecular dynamics cell and shape [91, 92]. The average volume is determined by the balance between the internal pressure and the externally set pressure. The enthalpy of the system is approximately conserved, so this method generates the constant enthalpy, constant pressure (HPN) ensemble. As a consequence, the Parrinello-Rahman scheme is particularly useful to study phase transitions in solids. In the Parrinello-Rahman formalism,

the edges of the MD cell are specified by three vectors $\vec{a}$, $\vec{b}$, $\vec{c}$ and which are time dependent. Periodically repeating MD cells fill up all space. The 3×3 matrix h is defined as the coordinates of $\vec{a}, \vec{b}, \vec{c}$. $\Omega_0 = det h_0 = \vec{a}.\vec{b} \times \vec{c}$ is then the volume of the MD cell containing the particles. The position of the particle i is given by $\vec{r}_i = \xi_i \vec{a} + \eta_i \vec{b} + \zeta_i \vec{c} = \underline{h} \vec{s}_i$, where $\vec{s}_i$ has components (ξ, η, ζ) each going from 0 to 1. Then the square of the distance between i and j is given by $r_{ij}^2 = (\vec{s}_i - \vec{s}_i)' \underline{G} (\vec{s}_i - \vec{s}_j)$, where G is the metric tensor, $\underline{G} = \underline{h}' h$, the transpose being denoted by a prime.

Nosé [89, 90] proposed a new MD method at constant temperature. The total energy of the physical system is allowed to fluctuate by the introduction of an additional degree of freedom, s. A special choice of the potential for the variable s guarantees that the averages of static quantities in this method are equal to those in the canonical ensemble (TVN). The total Hamiltonian is conserved and all the equation of motions are solved without introducing any stochastic process in the extended system of the particles and the coordinate s. This variable s can be interpreted as a scaling factor for the time step in the simulations.

Nosé [89, 90] has also showed how to formulate the constant temperature and constant pressure (TPN) ensemble in the form of the constant pressure simulation method by Andersen [88]. Later Hoover [93] has simplified the equations of motion derived by Nosé.

In this study, we use MD computer program whose algorithms based on extended Hamiltonian formalism emerging from the works of Andersen [88], Parrinello and Rahman [91, 92], Nosé [89, 90], Hoover [93] and Çağın [94]. The details of the computational procedure are described in the following section.

2.3   Computational Procedure

The simulation starts with 864 atoms in a cubic box randomly distributed on an fcc lattice subject to the periodic boundary conditions described in Section 2.4. The system is thermalised starting from 0.1 K to the target temperature using a constant enthalpy, constant pressure (HPN) ensemble by slowly heating while scaling velocities to increase the temperature by 1 K/step over the specific number of steps depending on the target temperature. The variation of the total energy with respect to MD steps as the temperature increases is given in the Fig. 2.1. As explicitly shown in the figure, total energy rises as MD steps go on. Then, this is followed by equilibration of the system at each target temperature. Fig. 2.2 shows the total energy calculated at 300 K in HPN ensemble as a function of MD steps. The system is equilibrated at this temperature by scaling the velocities. Total energy fluctuates around the equilibrium value. After that, the constant temperature-constant pressure ensemble (TPN) dynamics are performed for the production runs at this temperature for 20000 steps to calculate the volume, density and enthalpy of system for each concentration. The Fig. 2.3 shows the change of the total energy with respect to MD steps in TPN ensemble. The

total energy also fluctuates around the mean values. The resulting zero strain average matrix $< h_0 >$ is used to calculate pressure dependent properties of the system over 50000 steps of EVN dynamics. Fifth order Gear predictor-corrector algorithm, described in Section 2.5, is used with time integration step $\Delta t = 0.002$ ps. Parrinello-Rahman piston mass parameter is chosen as W=400 and the Nosé-Hoover parameter is set to Q=100. The interaction range of the potential is taken to be two lattice parameters. The temperature effects are taken into consideration by extending the range by an additional distance of half a lattice parameter.

The cooling process is mainly concerned with two main ensemble dynamics: constant temperature and constant pressure (TPN), and constant temperature and constant volume (TVN) MD simulations. The simulations are performed for three different simulation times; 20, 40, and 200 ps, corresponding to the cooling rates of 5.0 K/ps, 2.5 K/ps, and 0.5 K/ps, respectively. The system is cooled with different cooling rates from 3000 K to 100 K in 100 K decrements in TPN ensemble, after equilibrating the structure in liquid phase. Then some thermodynamical, structural, and dynamical properties are analyzed. TVN simulations are carried out by using the reference volume of the TPN simulation of each target temperature at three different simulation times in order to find the diffusion coefficients.

The necessary data from each ensemble simulation is stored as a time series of coordinates, kinetic, and potential energies to calculate the physical properties of the system. Thermodynamic properties of the system are calculated by taking
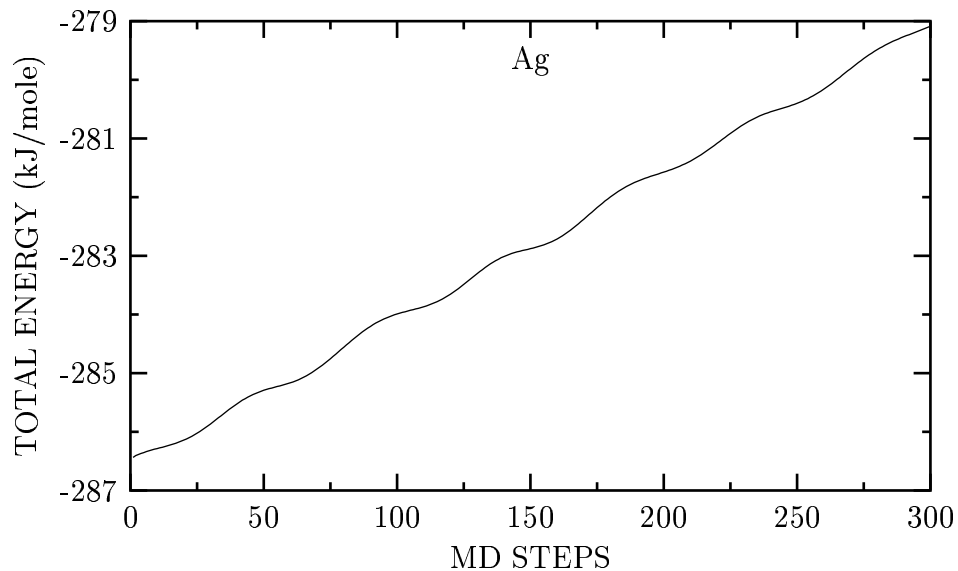
Figure 2.1: Evaluation of the total energy of Ag during a MD simulation for the heating processes in the HPN ensemble. Here the system is heated from 0 K to 300 K.
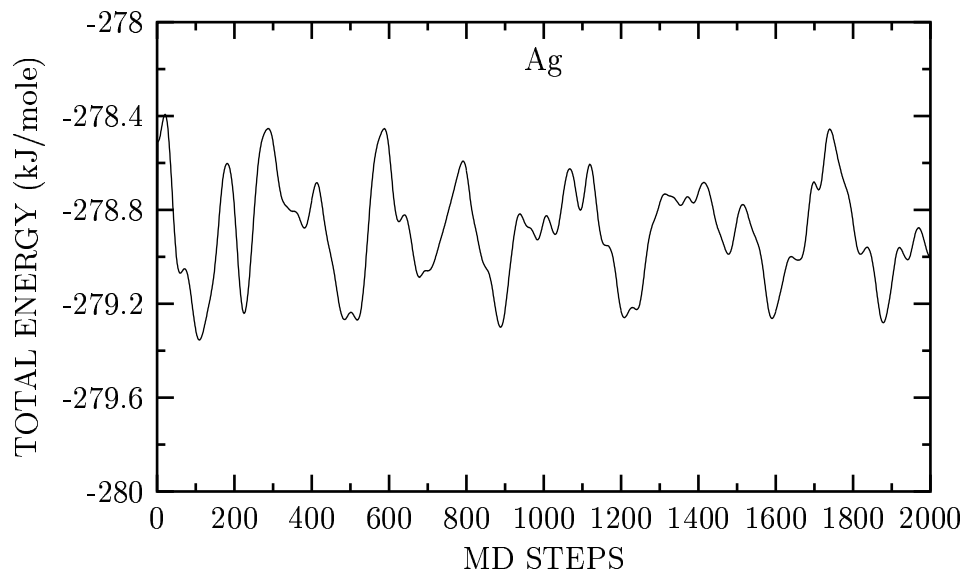
Figure 2.2: Equilibration of the total energy of Ag during a MD simulation time steps at 300 K in the HPN ensemble.
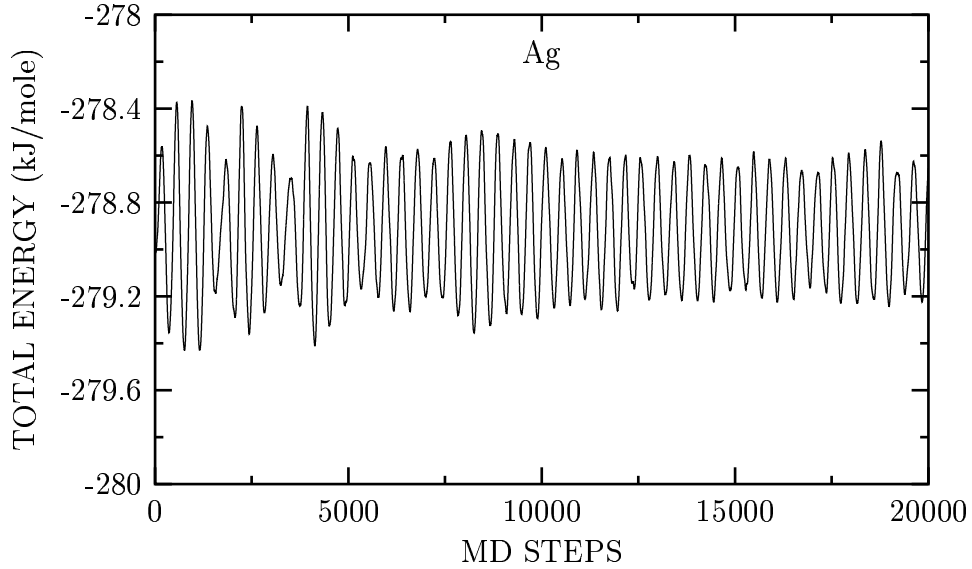
Figure 2.3: Time dependence of the total energy in the TPN ensemble.

the ensemble average. Time ensemble average can be computed for macroscopic

properties, for example $< A >$, as follows;

$$< A >= lim_{t \to \infty} \frac{1}{t} \int_{t_0}^{t_0+t} A(\tau)d\tau \qquad .\qquad (2.1)$$

MD also provides the structural quantities such as pair distribution function,

which gives the distribution of the distances between pairs of atoms, and structure

factor which is a Fourier transform of the pair distribution function. The structure

factor is measured in neutron-scattering experiments. MD is also one way to

calculate response functions which are obtained from time correlation functions

between two different quantities. Diffusion, viscosity, and dynamical structure

19

factor are the properties derived from the response functions.

2.4   Periodic Boundary Conditions

Most simulations probe the structural and thermodynamical properties of a system of a few hundred to a few thousand atoms. However, this number is still far away from the thermodynamical limit.

It is necessary to choose boundary conditions (pbc) that mimic the presence of an infinite bulk surrounding our N atoms of the system in order to simulate bulk phases.

In a simulation of N atoms confined to a volume V, we imagine that volume is only a small portion of the bulk material. The volume, V, is called the primary cell. It is representative of the bulk material the extent that the bulk is assumed to be composed of the primary cell surrounded by exact replicas of itself. Thus, the primary cell is imagined to be periodically replicated in all directions to form a macroscopic sample of the substance of interest. The problem of the surface effects can be overcome by implementing pbc. As an atom leaves the central box, its image enter through the opposite face of cell. Thus, the number of atoms in the primary cell is conserved [73, 75, 95, 96].

20

2.5 Time Evaluation of Atomic Positions and Gear's Predictor-Corrector Algorithms

A MD program requires good algorithms to integrate Newton's equation of motion. The choice of algorithm is important for different point of views. For example, speed of the program, accuracy, stability, and energy conservation depend directly on the algorithms. An algorithm should predict accurately the trajectory of all particles for both short and long times [95]. It should also be simple in form and easy to program. Such an algorithm is the Gear predictor-corrector algorithm. The drawbacks of this algorithm are the storage and the requirement for large memory. Since the trajectory of the atomic motion is a continuous function of time; position, velocity, and acceleration at time $t + \Delta t$ can be expanded as a Taylor series and predicted as follows [7, 73];

$$
\begin{aligned}
r_i^p(t + \Delta t) &= r_i(t) + \dot{r}_i(t)\Delta t + \frac{\ddot{r}_i(t)}{2!}(\Delta t)^2 + \frac{r_i^{(iii)}(t)}{3!}(\Delta t)^3 \\
&+ \frac{r_i^{(iv)}(t)}{4!}(\Delta t)^4 + \frac{r_i^v(t)}{5!}(\Delta t)^5 \quad ,
\end{aligned} \tag{2.2}
$$

$$
\begin{aligned}
\dot{r}_i^p(t + \Delta t) &= \dot{r}_i(t) + \ddot{r}_i(t)\Delta t + \frac{r_i^{(iii)}(t)}{2!}(\delta t)^2 + \frac{r_i^{(iv)}(t)}{3!}(\Delta t)^3 \\
&+ \frac{r_i^{(v)}(t)}{4!}(\Delta t)^4 \quad ,
\end{aligned} \tag{2.3}
$$

$$
\ddot{r}_i^p(t + \Delta t) = \ddot{r}_i(t) + r_i^{(iii)}(t)\Delta t + \frac{r_i^{(iv)}(t)}{2!}(\Delta t)^2 + \frac{r_i^{(v)}(t)}{3!}(\Delta t)^3 \quad , \tag{2.4}
$$

21

$$r_i^{(iii)p}(t + \Delta t) \;=\; r_i^{(iii)}(t) + r_i^{(iv)}(t)\Delta t + \frac{r_i^{(v)}(t)}{2!}(\Delta t)^2 \quad , \tag{2.5}$$

$$r_i^{iv}(t + \Delta t) \;=\; r_i^{iv}(t) + r_i^{(v)}(t)\Delta t \quad , \tag{2.6}$$

$$r_i^{(v)p}(t + \Delta t) \;=\; r_i^{(v)}(t) \quad . \tag{2.7}$$

The force acting on the atoms can be calculated at time $t + \Delta t$ by using the new predicted position $r_i^p(t + \Delta t)$, and the acceleration $a_i^C(t + \Delta t)$ can be used as a corrector. The discrepancy between the predicted and observed accelerations can be used to improve estimation of the position and the remaining derivatives. This is the 'corrector' part of the predictor-corrector algorithm. The error in the predicted acceleration, $a_i^p(t + \Delta t)$, is given as follows;

$$\Delta a_i(t + \Delta t) = a_i^c(t + \Delta t) - a_i^p(t + \Delta t) \quad . \tag{2.8}$$

Adding this difference to the predicted values, the corrected quantities can be given as;

$$r_i^c(t + \Delta t) \;=\; r_i^p(t + \Delta t) + c_0 \Delta a_i(t + \Delta t) \quad , \tag{2.9}$$

$$\dot{r}_i^c(t + \Delta t) \;=\; \dot{r}_i^p(t + \Delta t) + c_1 \Delta a_i(t + \Delta t) \quad , \tag{2.10}$$

$$\ddot{r}_i^c(t + \Delta t) \;=\; \ddot{r}_i^p(t + \Delta t) + c_2 \Delta a_i(t + \Delta t) \quad , \tag{2.11}$$

22

$$r_i^{(iii)c}(t + \Delta t) \quad = \quad r_i^{(iii)p}(t + \Delta t) + c_3 \Delta a_i(t + \Delta t) \quad , \quad (2.12)$$

$$r_i^{(iv)c}(t + \Delta t) \quad = \quad r_i^{(iv)p}(t + \Delta t) + c_4 \Delta a_i(t + \Delta t) \quad , \quad (2.13)$$

$$r_i^{(v)c}(t + \Delta t) \quad = \quad r_i^{(v)p}(t + \Delta t) + c_5 \Delta a_i(t + \Delta t) \quad . \quad (2.14)$$

In this study, we use the fifth order Gear predictor-corrector algorithm. Gear has determined the coefficients (c_i, i=1,... 5) such that they yield optimal compromise between the accuracy and stability of the algorithm [97]. The coefficients are given in Table 2.1

Table 2.1: Values of c_i parameters in fifth order Gear's Predictor-corrector Algorithm.

c_0	c_1	c_2	c_3	c_4	c_5
3/20	251/360	1	11/18	1/6	1/60

The above descriptions are used for the microcanonical (EVN) simulation, where the total energy is a conserved quantity. We wish to keep the temperature or pressure constant to perform simulations in the other ensembles such as TPN, TVN and HPN. In such cases, since integrating Newton's equation of motion is not enough, one needs to add the effect of the thermostat interacting with the system as done in the Nosé method [89, 90].

23

2.5.1 How to Choose the Integration Time Step, Δt

There is no strict rules for selecting the most appropriate time step to use in MD simulation. If it is too small, the trajectory covers only a limited portion of the phase space, and if it is too large, instability may occur in the integration algorithm due to high energy overlaps between atoms. Such instability and inaccuracy lead to a violation of energy and linear momentum conservation and result in a program failure due to numerical overflow. The aim is to find the correct balance between simulating the correct trajectory and covering the phase space.

When simulating an atomic system the time step should be small compared to the mean time between collisions. The time step may be taken approximately one tenth of the time of the shortest period of motion. More details for choosing an integration time step can be found in Ref. [96].

2.6 Limitations of Classical Molecular Dynamics

MD is limited largely by the speed and storage constraints of available computers. The main limitations of the MD are mainly in the size of the system containing thousands-millions of atoms and simulation time ranging from a few picoseconds to hundreds of nanoseconds. Several tens of thousands of particles can be handled with the rapidly growing computer memory [98]. Time limitation also indicates a limit in the configurational sampling that can be achieved by MD. Sufficient sampling of the configurational space accessible in an equilibrium condition is essential for computing the thermodynamic properties. The systems

at the atomistic level obey quantum laws rather than classical laws. Moreover quantum effects become important in any system when temperature is sufficiently low.

CHAPTER 3

INTERATOMIC POTENTIALS

3.1 Introduction

Computer simulations are becoming an integral part of many investigative procedures and provide help in understanding various problems at the atomistic level. The computer simulation techniques are mostly based on interatomic model potential governing interactions among the atoms of the system. Computationally most efficient method is the use of interatomic potential for model systems composed of several hundred to several million atoms. This potential function describes how the potential energy of a system of N atoms depends on the coordinates of the atoms. The concept of model potential is based on the Born-Oppenheimer approximation if it is assumed that in the absence of external forces, the total energy of a system of N interacting particles may be written as [10];

$$U_{tot}(r_1, r_2, ...r_N) = \sum_i U_1(r_i) + \sum_i \sum_{j>i} U_2(r_{ij}) + \sum_i \sum_{j>i} \sum_{k>j} U_3(r_i, r_j, r_k) + ... \quad (3.1)$$

where U_1 is the one-body term due to an external field, U_2 is the two-body, or pair potential, U_3 is the three-body term which arises when the interaction of a pair

26

of atoms is modified by the presence of a third atom. Based on this expansion, interatomic potentials are classified into two classes: pair potential (only U_1 and U_2 is present) and many-body potentials (U_3 and higher terms are included).

3.2   Problem with Two-Body Potentials

Total potential energy is approximated only by the sum of two-body interaction in the earlier calculations. This approach not only simplifies the statistical formalism used in calculating various thermodynamical properties but also it enabled many earlier researchers to simulate with relatively smaller and less powerful computers. The predominant forces arise from the van der Walls interaction, especially in the metallic case, which are responsible for long-range cohesion for large inter-atomic distances. Metallic bonding is due to the sharing of the electrons in the system and hence a proper description of this bonding requires the consideration of the many-body effects. The pair-wise potentials are insufficient to define metallic bonding for following reasons [2, 3, 12, 13, 14];

1-The ratio of the elastic constants C_{12}/C_{44} is far from 1, whereas a pair-wise potential leads to the Cauchy relation $C_{12} = C_{44}$.

2- Prediction of the un-relaxed vacancy formation energy gives values around the cohesive energy. Experimental data suggest that the vacancy formation energy for metals is about one third of the cohesive energy.

3- Pair potentials fail to predict an inward relaxation of the metallic surfaces.

4- Pair-wise potentials overestimate the melting point by up to 20 % of the

experimental value.

A significant progress was made to overcome these drawbacks during the 80's by the development of many-body potentials for metals based on the concept of density, coordination, as the key variable to consider. There are several available potentials in literature that mimic the many-body effects. These potentials are the embedded-atom model (EAM) [12, 99], which has been employed in several studies involving elemental metals and their alloys [100], Glue Model [101], the Finnis Sinclair (FS) potentials for the bcc elemental metals [13], which have also been developed for the noble metals [61], the Sutton Chen (SC) potentials [15] for the ten fcc elemental metals, and the Rafii-Tabar and Sutton potentials [102] for the fcc random binary alloys which have also been used in several modeling studies [25, 103, 104, 105, 106].

We have used SC type potentials in this study because of long range properties and computational efficiency. These potentials are in the same form of the FS type potentials. Hence, it is convenient to describe a background for SC type potentials.

3.3   Finnis-Sinclair Potential

The FS potentials are constructed to model the energetics of the bcc transition metals. In the FS model, the total energy of an N atom system is written as [13];

$$U_{tot} = \frac{1}{2} \sum_i^N \sum_{j \neq i} V(r_{ij}) - c \sum_i \sqrt{\rho_i} \qquad , \qquad (3.2)$$

where

$$\rho_i = \sum_{j \neq i} \phi(r_{ij}) \qquad .\qquad (3.3)$$

The function $V(r_{ij})$ is a pair-wise repulsive interaction between atoms i and j separated by a distance r_{ij}, $\phi(r_{ij})$ is a two-body cohesive part of potential and c is a positive constant. The second term in Eq. 3.2 represents the cohesive many-body contribution to the energy. The square root form of this term was motivated by an analogy with the second moment approximation to the tight binding model (SMA-TBM) [61]. In this approximation, cohesive energy of a solid scales with the square root of its atomic coordination number [15]. The function $\phi(r_{ij})$ can be interpreted as the sum of squares of hopping (overlap) integrals. The function ρ_i may be interpreted as the local electronic charge density at site i which is constructed by a rigid superposition of atomic charge densities [99]. In this interpretation, the energy of an atom at site i is assumed to be the same as if it were in a uniform electron gas of that density. Alternatively, ρ_i can be interpreted as a measure of the local density of atomic sites [13]. The Eq. 3.2 is then interpreted as the sum of the volume-dependent energy U_N, represented by the second term and the pair-wise summation U_p, represented by the first term. This FS potential has been generalised to several alloy systems, such as the alloys of the noble metals [102].

3.4 Sutton-Chen Potential

SC many-body potentials are of the FS type and similar in form to the Embedded Atom Model (EAM) [12]. They consist of a pair-wise term and a term proportional to the square root of the local density which represents the cohesive energy resulting from electrons. These potentials have been generalized to model the interaction of unlike atoms in fcc random binary metallic alloys by Rafii-Tabar and Sutton [102]. The general form of the total potential energy of the metals and alloys in this formalism is given as follows [15, 102, 104];

$$U_{tot} = \sum_i U_i = \sum_i \left[\sum_{i \neq j} \epsilon_{ij} \frac{1}{2} V(r_{ij}) - c_i \epsilon_{ii} (\rho_i)^{\frac{1}{2}} \right] \quad , \tag{3.4}$$

where $V(r_{ij})$ is a pair potential defined by

$$V(r_{ij}) = (\frac{a_{ij}}{r_{ij}})^{n_{ij}} \quad , \tag{3.5}$$

accounting for the repulsion between the i and j atomic cores and ρ_i is a local density accounting for the cohesion associated with atom i which is defined as follows;

$$\rho_i = \sum_{i \neq j} \phi(r_{ij}) \quad , \tag{3.6}$$

where

$$\phi(r_{ij}) = \left(\frac{a_{ij}}{r_{ij}} \right)^{m_{ij}} \quad . \tag{3.7}$$

In Eqs.(3.4)-(3.7), r_{ij} is the distance between atoms i and j, a_{ij} is a length parameter, c is a dimensionless parameter scaling the attractive term to repulsive term, ϵ sets the overall energy scale, and n, m are integer parameters with $n > m$.

To extend the potential parameters to alloys, we use the following combination rules to represent the interactions between Pd-Ag and Cu-Au pairs, even though there are different cases we prefer to use the combination rules and demonstrate their applicability in this study;

$$\epsilon_{ij} \ = \ (\epsilon_i \epsilon_j)^{\frac{1}{2}} \quad , \tag{3.8}$$

$$m_{ij} \ = \ \frac{(m_i + m_j)}{2} \quad , \tag{3.9}$$

$$n_{ij} \ = \ \frac{(n_i + n_j)}{2} \quad , \tag{3.10}$$

$$a_{ij} \ = \ \frac{(a_i + a_j)}{2} \quad . \tag{3.11}$$

Recently, Çağın and co-workers [74] have reparametrized the empirical many-body force field of the SC type for the face-centered cubic (fcc) metals by fitting to 0 K experimental properties such as density, cohesive energy, moduli, and phonon frequencies at the X point (at room temperature) while including the zero-point energy (thus it is called quantum). They have employed this potential in a series of important problems in metal physics [25, 105, 106, 107, 108, 109, 110, 111, 112, 113, 114].

SC potential does not describe well the properties involving defects, surfaces and interfaces since the potential parameters are based only on the experimental lattice constant, cohesive energy and bulk modulus [15]. However, Q-SC potential includes the quantum correction to take into account the zero-point energy. This potential allows one to do a more accurate calculation of the temperature dependence of various physical properties.

The SC interaction potential has been adopted by Rafii-Tabar and Sutton [102] to describe the random fcc alloy model in which sites are occupied by two types of atoms completely randomly, such that the alloy has the required average concentration. No relaxation of the atomic positions is considered. They have recomputed potential parameters for a cut-off radius of two lattice parameters. The modified SC potential [102] and Q-SC potential parameters [74] for Pd, Ag, Cu, and Au metals are given in the Table 3.1.

Table 3.1: Q-SC and SC potential parameters for Pd, Ag, Cu, and Au.

metal		n	m	$\epsilon(eV)$	c	$a(A^0)$
Pd	Q-SC	12	6	3.2864E-3	148.205	3.8813
	SC	12	7	4.1260E-3	108.526	3.8900
Ag	Q-SC	11	6	3.9450E-3	96.524	4.0691
	SC	12	6	2.5330E-3	145.658	4.0900
Cu	Q-SC	10	5	5.7921E-3	84.8430	3.60300
	SC	9	6	1.23860E-2	39.75500	3.61530
Au	Q-SC	11	8	7.8052E-3	53.58100	4.06510
	SC	10	8	1.27940E-2	34.4280	4.07830

CHAPTER 4

RESULTS AND DISCUSSION

4.1 SOLID PROPERTIES

4.1.1 Enthalpy of Mixing

Enthalpy of mixing ΔH is calculated to trace the behavior of Pd-Ag alloy system at different temperatures. ΔH, per atom, at 0 K and finite temperatures, may also be calculated from

$$\Delta H = E^t - c_A E^A - c_B E^B \qquad , \tag{4.1}$$

where E^A and E^B are the cohesive energies per atom of the elemental A and B metals and the constants are such that $c_A + c_B = 1$.

The result is shown in Fig. 4.1. The sign of experimental data at 1200 K [115] agrees with the theoretical data at 1300 K. The experimental data for other temperatures are not available in the literature to verify the results for enthalpy of mixing at elevated temperatures. The enthalpy of mixing is particularly sensitive to whether local relaxation is allowed, as pointed by Ackland and Vitek [61] and Rafii-Tabar and Sutton [102]. In addition to ignoring local relaxation, the enthalpies calculated are valid only at 0 K because the temperature dependence
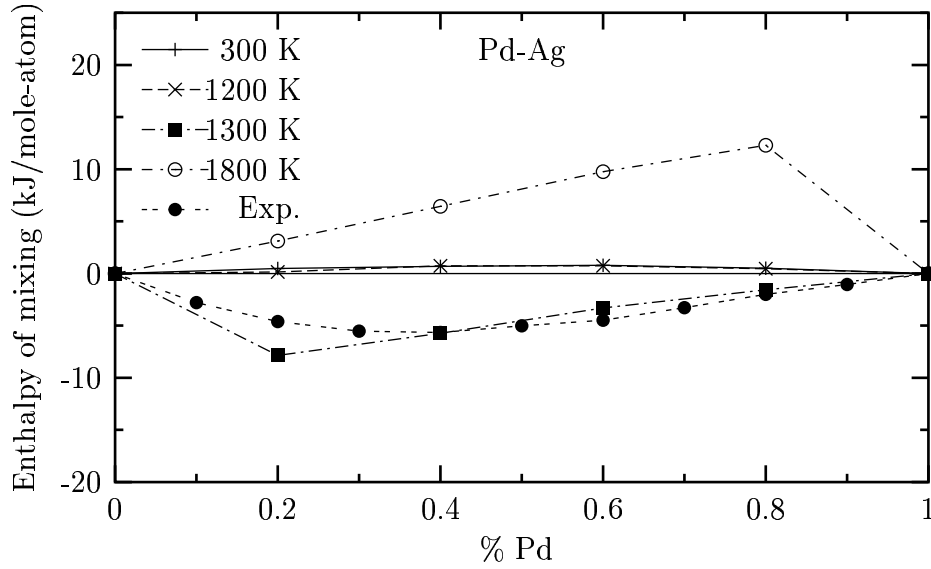
Figure 4.1: Enthalpy of mixing ΔH for Pd-Ag system at different temperatures along with experimental data at 1200 K [115].

of enthalpy of mixing is ignored. Another drawback of the calculation may come from random-alloy model rather than our potentials. The results may be improved by optimizing the initial configuration for the positions of Pd and Ag atoms in the Pd-Ag system by using Monte Carlo simulations.

4.1.2 Mechanical and Thermodynamical Properties

The results for the calculation of the lattice constant, cohesive energy, density, elastic constants and bulk modulus of Pd, Ag and Pd-Ag for both Q-SC and SC potentials are presented in Tables 4.1 and 4.2 with the experimental data

(whenever available) and other theoretical calculations. These solid properties are calculated at different temperatures and concentrations. Here, we only give solid properties obtained from Q-SC and SC potential parameters at the specific temperatures of 0 K and 300 K in order to compare with the experimental data. Our calculations are in good agreement with the experimental results [116] and other theoretical calculations [15, 117] although there are small discrepancies.

4.1.2.1 Elastic Constant, Bulk Modulus and Compressibility

We have calculated the elastic constants for Pd-Ag system by using the following statistical fluctuation expression [103, 104, 118].

$$
\begin{aligned}
C_{\alpha\beta\gamma\kappa} = \frac{\Omega_0}{k_B T} \left(<P_{\alpha\beta}P_{\gamma\kappa}> - <P_{\alpha\beta}><P_{\gamma\kappa}> \right) \\
+ \frac{2Nk_B T}{\Omega_0} \left(\delta_{\alpha\gamma}\delta_{\beta\kappa} + \delta_{\alpha\kappa}\delta_{\beta\gamma} \right) + <\chi_{\alpha\beta\gamma\kappa}> \qquad ,
\end{aligned}
\tag{4.2}
$$

where angular brackets denote the averaging over time and $\Omega_0 = deth_0$ is the reference volume for the model system. The first term represents the contribution from the fluctuation of the microscopic stress tensor $P_{\alpha\beta}$, the second term designates the kinetic energy contribution, and the third term is the Born term. The anisotropic stress tensor including the contribution from the many body potential is calculated from;

$$
\Omega P_{\alpha\beta} = \sum_i \frac{P_{i\alpha}}{j\beta} m_i - \frac{\epsilon_{ij}}{2} \sum_i \left(\sum_j V'(r_{ij}) \frac{r_{ij\alpha}r_{ij\beta}}{r_{ij}} - c_i \frac{\sum_j \phi(r_{ij})'(r_{ij\alpha}r_{ij\beta}/r_{ij})}{\rho_i} \right)
\tag{4.3}
$$

The potential energy contribution to the elastic constants, the hypervirial tensor, $\chi_{\alpha\beta\gamma\kappa}$, is given as;

$$\Omega \chi_{\alpha\beta\gamma\kappa} = \frac{\epsilon_{ij}}{2} \sum_i \left\{ \sum_j (V'' - \frac{V'}{r_{ij}}) \frac{r_{ij\alpha} r_{ij\beta} r_{ij\gamma} r_{ij\kappa}}{r_{ij}^2} \right.$$

$$- \ c_i \frac{\sum_j (\phi'' - \frac{\phi'}{r_{ij}})(r_{ij\alpha} r_{ij\beta} r_{ij\gamma} r_{ij\kappa}/r_{ij}^2)}{\rho_i} \qquad (4.4)$$

$$+ \ \frac{c_i}{2} \frac{\left[\sum_j \phi'(r_{ij\alpha} r_{ij\beta}/r_{ij}) \right] \left[\sum_k \phi'(r_{ik\gamma} r_{ik\kappa}/r_{ik}) \right]}{\rho_i^3} \left. \right\} \qquad .$$

The symmetry averaged values for the nine components of the elastic constants computed from both SC and Q-SC parameters are obtained at most with an error of 0.03 %. Elastic constants and bulk moduli which are especially computed from SC potential parameters for Pd and Ag are quite close to the experimental values, as shown in the Table 4.1. The ratio of C_{12}/C_{44} evaluated from Q-SC is 1.72 (2.44) for Pd, 1.77 for $Pd_{0.8}Ag_{0.2}$, 1.79 for $Pd_{0.6}Ag_{0.4}$, 1.85 for $Pd_{0.4}Ag_{0.6}$, 1.87 for $Pd_{0.2}Ag_{0.8}$, and 1.89 (2.05) for Ag, where the numbers in parentheses are experimental values from the Ref. [119]. On the other hand, the ratios of C_{12}/C_{44} for Pd and Ag by using SC parameters are 1.99 and 1.75, respectively. The ratio for Pd calculated from SC potential parameters is closer to the experimental value than that from Q-SC. The same behavior for Ag, however, is not seen. The results for the elastic constants of pure and alloy systems show that the crystals are mechanically stable since the stability conditions $C_{44} > 0$, $C_{11} > 0$ and $C_{11} > C_{12}$ are satisfied.

Figs 4.2-4.4 are given to show the effects of the concentration on the elastic constants, bulk modulus, and compressibility at 300 K and 700 K. The variations

Table 4.1: Elastic constants and bulk moduli of Pd, Ag and Pd-Ag alloys at 0 K and 300 K along with the available experimental and theoretical data. Elastic constants and bulk moduli are in units of GPa. Bulk moduli are calculated from the expression of $B=(C_{11}+2\ C_{12})/3$.

	T(K)		C_{11}	C_{12}	C_{44}	B
Pd	0	Q-SC	217.30	149.68	91.60	172.22
	300	Q-SC	202.66	140.69	81.99	160.96
	0	SC	248.20	175.91	93.30	200.01
	300	SC	229.48	164.45	82.72	186.22
	0	Exp. [116]	234.10	176.10	71.20	195.43
	300	Exp. [116]	227.10	176.10	71.70	180.80
		Ref. [15]	248.30	176.20	92.90	200.20
		Ref. [117]	232	178	74	
$Pd_{0.8}Ag_{0.2}$	300	Q-SC	181.51	127.30	71.85	145.09
$Pd_{0.6}Ag_{0.4}$	300	Q-SC	162.07	114.66	63.74	130.45
$Pd_{0.4}Ag_{0.6}$	300	Q-SC	145.08	103.69	56.01	117.16
$Pd_{0.2}Ag_{0.8}$	300	Q-SC	130.06	93.21	49.82	105.76
$Pd_{0.0622}Ag_{0.9378}$	300	Q-SC	120.96	86.87	46.08	98.23
	300	SC	131.12	92.07	51.80	105.80
	300	Exp. [120]	127.70	95.80	48.10	106.43
Ag	0	Q-SC	128.73	91.39	52.03	103.84
	300	Q-SC	116.29	83.87	44.39	94.42
	0	SC	139.78	96.71	59.13	111.04
	300	SC	126.49	88.32	50.51	101.02
	0	Exp. [119]	131.50	97.30	51.10	108.70
	300	Exp. [119]	124.00	93.70	46.10	100.70
		Ref. [15]	140.99	96.13	59.3	110.54
		Ref. [117]	132	97	51	108

between the elastic constants and concentration of Pd show nearly a linear dependence. Increasing the concentration of Pd in Pd-Ag alloys leads to increase in the elastic constant and bulk modulus, while decrease in the compressibility, as expected.

4.1.2.2   Lattice Parameter, Cohesive Energy, and Density

The lattice parameters, cohesive energy and density calculated from SC and Q-SC potential parameters are in good agreement with the experimental and theoretical calculations. Generally, the results obtained from Q-SC potential parameters are closer to the experimental data. Q-SC potential parameters give rise to improvements over SC potential parameters, as shown in Table 4.2. We have calculated lattice parameter, cohesive energy, density and elastic constants for the $Pd_{0.0622}Ag_{0.9378}$ alloy case so as to compare with the available experimental data. Density and elastic constants computed from both potential parameter sets are compatible with the available experimental data although there is a small discrepancy, as shown in Tables 4.1 and 4.2. It may be concluded that Rafii-Tabar's random alloy model generate useful information about the alloy system without further empirical fitting to properties of Pd_xAg_{1-x}.

4.1.3   Phonon Dispersion Curves

In the classical picture within the harmonic approximation the atoms of a crystal are visualized as joined by harmonic springs and crystal dynamics is analyzed in terms of a linear combination of $3n$ normal modes of vibration. The
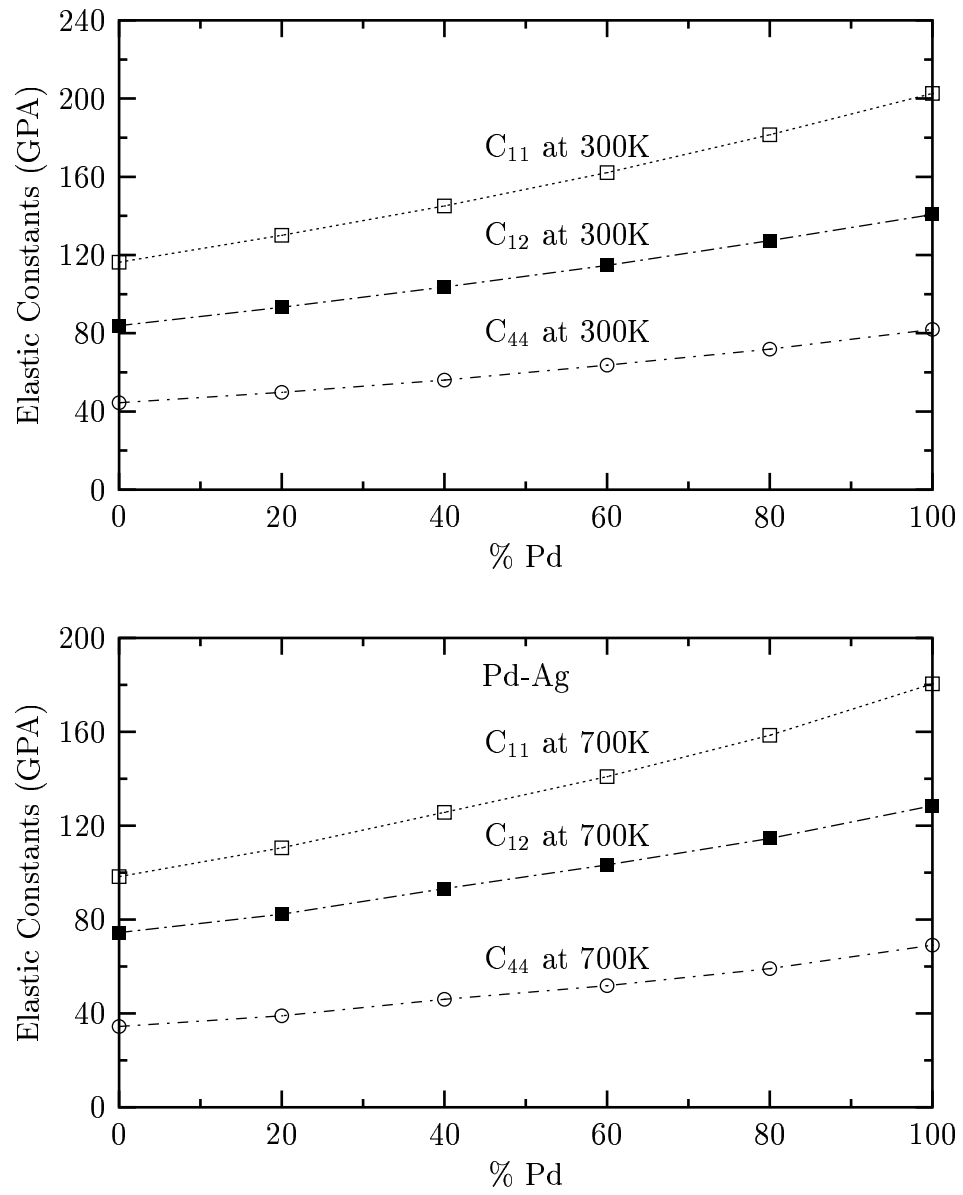
Figure 4.2: The elastic constants of Pd-Ag alloys as a function of concentration of Pd in Ag at two different temperatures.
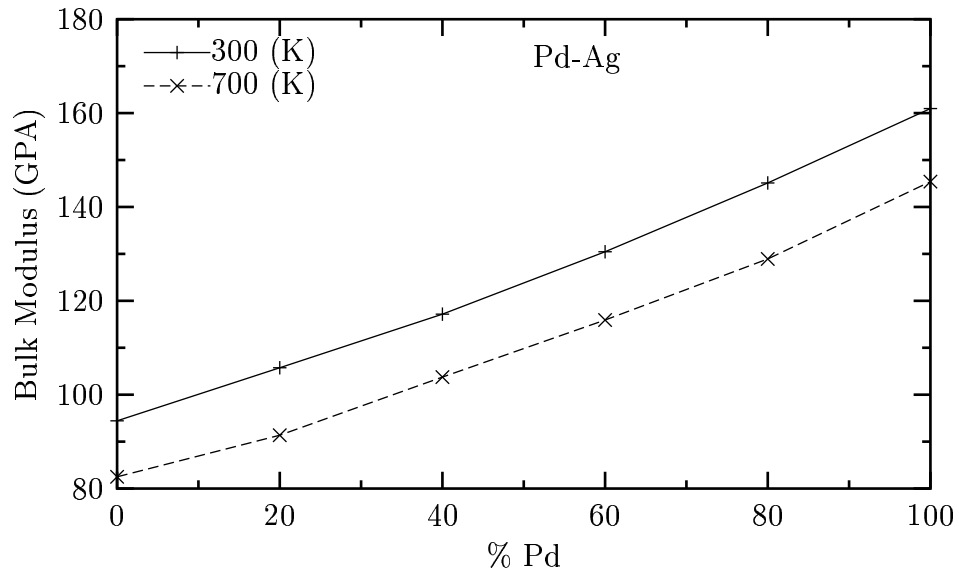
Figure 4.3: The bulk modulus as a function of concentration of Pd in Ag at 300 K and 700 K.
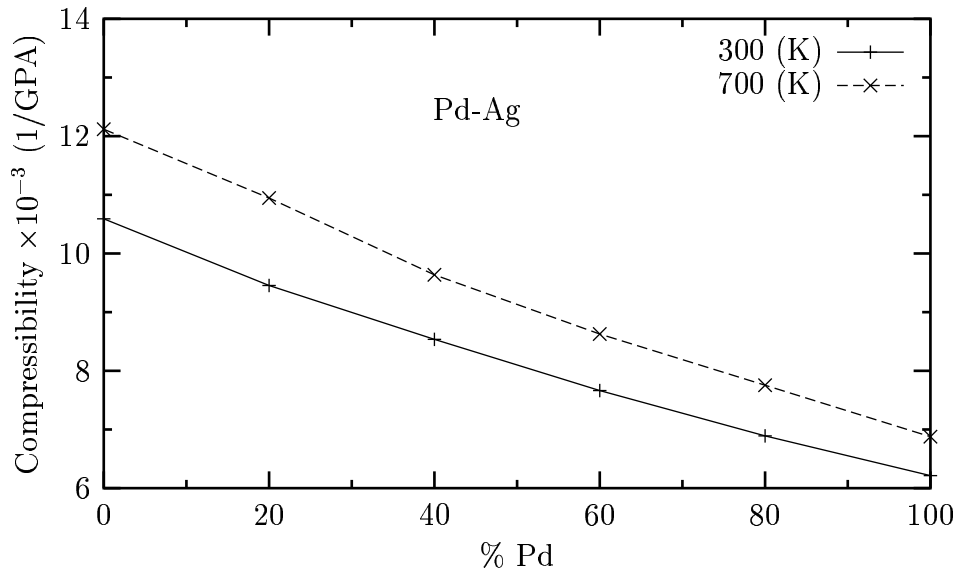
Figure 4.4: The compressibility as a function of concentration of Pd in Ag at 300 K and 700 K.

Table 4.2: Lattice parameter a, cohesive energy E_c, and density ρ of Pd, Ag and Pd-Ag alloys at 0 K and 300 K along with the available experimental and theoretical data.

	T(K)		a(A^0)	E_c(kJ/mole)	ρ(g/cm^3)
Pd	0	Q-SC	3.874	377.90	12.16
	300	Q-SC	3.896	370.24	11.95
	0	SC	3.890	380.10	12.00
	300	SC	3.911	372.51	11.81
	0	Exp. [116]		376.	12.13
	300	Exp. [116]	3.89		12.00
		Ref. [15]	3.89	380.15	
		Ref. [117]	3.889	379.77	
$Pd_{0.8}Ag_{0.2}$	300	Q-SC	3.933	351.48	11.65
$Pd_{0.6}Ag_{0.4}$	300	Q-SC	3.971	332.93	11.34
$Pd_{0.4}Ag_{0.6}$	300	Q-SC	4.010	314.76	11.05
$Pd_{0.2}Ag_{0.8}$	300	Q-SC	4.051	296.71	10.75
$Pd_{0.0622}Ag_{0.9378}$	300	Q-SC	4.080	284.20	10.541
	300	SC	4.103	283.25	10.364
	300	Exp. [120]			10.606
Ag	0	Q-SC	4.061	286.55	10.69
	300	Q-SC	4.093	278.917	10.44
	0	SC	4.086	285.56	10.50
	300	SC	4.116	277.86	10.270
	0	Exp. [119]		284.	10.635
	300	Exp. [119]	4.06		10.50
		Ref. [15]	4.09	285.60	

41

energies of normal modes of a crystal are quantized. Phonon is a quantum of crystal vibrational energy.

The problem of lattice dynamics in the harmonic approximation is to find the normal modes of a crystal, in other words, we seek to calculate the phonons as a function of their wave vector $\mathbf{q}$. The relationship between w and q, namely $w = w(\mathbf{q})$, is called the phonon dispersion. The dispersion curves shows the translational symmetry in q space [121, 122].

A crystal is composed of an infinite number of unit cells, each of which has n atoms. The number of degrees of freedom will be 3n which is also the number of branches in the dispersion relation $w(\mathbf{q})$. Three of the branches are always acoustic and the rest of the branches are the optical branches. Two third of the branches are for transverse polarization and the rest is for longitudinal polarization.

Phonon dispersion curves $w(\mathbf{q})$ can be measured by inelastic neutron scattering techniques. The curves determined by experiments are mainly of interest because they provide a chance for testing various models of interatomic forces. Certain bulk properties of a crystal, such as the specific heat, are determined by an average over the whole phonon spectrum. This means that while the specific heat can be predicted when the $w(\mathbf{q})$ relation is known, the converse does not hold [123].

The dynamical matrix is given as [124];

$$D_{\alpha,\beta}(i,j,\mathbf{q}) = \frac{1}{(m_i m_j)^{\frac{1}{2}}} \sum_l \Phi_{\alpha\beta}(i,j,0,l) \, exp \, (i\mathbf{q}.[\mathbf{r}(j,l) - \mathbf{r}(i,0)]) \qquad , \qquad (4.5)$$

where $l = 0$ is the reference unit cell, l are the neighboring cell numbers. i, j are index of atoms in the unit cells, $\alpha, \beta = 1, 2, 3$ representing x, y, z, respectively. $D_{\alpha,\beta}(i,j,\mathbf{q})$ is the 3n×3n dynamical matrix and Φ is the force constant which can be calculated by taking the first derivative of the many-body force. The many-body force acting on atom i along a direction $\alpha(= x, y, z)$ is given as;

$$F_{i\alpha} = -\epsilon \left[\sum_{i \neq j} V'(r_{ij}) \frac{r_{ij\alpha}}{r_{ij}} - \frac{c}{2} \sum_{i \neq j} \frac{\phi'(r_{ij\alpha})}{\rho_i} \frac{r_{ij\alpha}}{r_{rij}} + \frac{c}{2} \sum_{i \neq j} \frac{\phi(r_{ij})}{\rho_j} \frac{r_{ji\alpha}}{r_{ji}} \right] \qquad , \qquad (4.6)$$

where the prime denotes differentiation with respect to r_{ij} and $r_{ij\alpha}$ denotes the calculated force on the i th atom in the α direction. The force constant is given as follows;

$$
\begin{aligned}
\Phi_{\alpha\beta}(i,j) = \quad &- \quad \epsilon \left[\left(V_{ij}'' - V_{ij}' \right) \Delta r_{ij\alpha} \Delta r_{ij\beta} + V_{ij}' \frac{\delta_{\alpha\beta}}{r_{ij}^2} \right] \\
&- \quad \frac{\epsilon c}{4\rho_i^{3/2}} \left(\sum_{k \neq i} \phi_{ik}' \Delta r_{ik\alpha} \right) \phi_{ij}' \Delta r_{ij\beta} \\
&+ \quad \frac{\epsilon c}{2\rho_i^{1/2}} \left[\left(\phi_{ij}'' - \phi_{ij}' \right) \Delta r_{ij\alpha} \Delta r_{ij\beta} + \phi_{ij}' \frac{\delta_{\alpha\beta}}{r_{ij}^2} \right] \\
&+ \quad \frac{\epsilon c}{4\rho_j^{3/2}} \phi_{ij}' \Delta r_{ij\alpha} \left(\sum_{k \neq j} \phi_{jk}' \Delta r_{jk\beta} \right) \qquad\qquad (4.7) \\
&+ \quad \frac{\epsilon c}{2\rho_j^{1/2}} \left[\left(\phi_{ij}'' - \phi_{ij}' \right) \Delta r_{ij\alpha} \Delta r_{ij\beta} + \phi_{ij}' \frac{\delta_{\alpha\beta}}{r_{ij}^2} \right] \\
&+ \quad \frac{1}{4} \sum_{k \neq i,j} \left[\frac{\epsilon c}{\rho_k^{3/2}} \left(\phi_{ik}' \Delta r_{ik\alpha} \phi_{jk}' \Delta r_{jk\beta} \right) \right] \qquad .
\end{aligned}
$$

43

In the harmonic approximation, the force constants have very simple physical meaning. Suppose that all atoms are at their equilibrium positions except for the atom j which is displaced an unit distance d_β in the β direction. In this case, the force applied on ith atom;

$$F_\alpha(i) = -\Phi_{\alpha\beta}(i, j) d_\beta \quad . \tag{4.8}$$

It follows that the coefficient $\Phi_{\alpha\beta}(i, j)$ is the negative force exerted in the α-direction on the atom i when the atom j is displaced a unit distance in the β-direction, while all other atoms are kept at their equilibrium position. In the expression (4.7) of the force constants, the order of differentiation can be interchanged without changing the value of the force constants. Therefore, the force constants satisfy the following symmetry condition;

$$\Phi_{\alpha\beta}(i, j) = \Phi_{\alpha\beta}(j, i) \quad . \tag{4.9}$$

In addition to this symmetry condition, the total force constant must vanish, that is, we obtain the following expression;

$$\sum_i \Phi_{\alpha\beta}(i, j) = 0 \quad . \tag{4.10}$$

It follows that diagonal force constant $\Phi_{\alpha\beta}(i, i)$ is not second derivative of the potential energy function but its components can be evaluated from the following relation;

$$\Phi_{\alpha\beta}(i, i) = -\sum_{j\neq i} \Phi_{\alpha\beta}(i, j) \quad . \tag{4.11}$$

44

Our cubic system is composed of 864 atoms, that is 216 unit cells. We choose the reference unit cell in the center of the cubic system after labeling all the atoms. We calculate the force constants by using the trajectories of Pd at 120 K and Ag at 300 K in the EVN dynamics. Then, we construct the dynamical matrix using the force constants and positions of atoms. The eigenvalues are computed by diagonalizing the dynamical matrix by using EISPACK or LAPACK subprogram. The order of force constants and that of phonon frequencies calculated are in agreement with the theoretical and experimental values. The phonon dispersion curves of Pd at 120 K and Ag at 300 K for Q-SC and SC potential parameters are shown in Figs. 4.5 (a) and (b) together with experimental data, respectively. The overall structure of dispersion curves are well reproduced. The low-frequency transverse modes computed both from Q-SC and SC potential parameters for Pd are found in agreement with experiment. The longitudinal higher frequency modes at X(L) for Pd are slightly smaller than the experimental data. On the other hand, the dispersion curves obtained from SC potential parameters for Ag at 300 K are consistent with the experimental values. Phonon dispersion curves calculated from Q-SC potential parameters for Ag are in good agreement with the experimental and SC potential parameters results.

While the Q-SC and SC phonon dispersion curves for Pd are consistent with each other, the improvement of Q-SC over SC potential for Ag is observed at the transverse acoustic modes as expected. This is due to fitting of Q-SC parameters to phonon frequencies at the X point. Here it may be noted that original SC

45
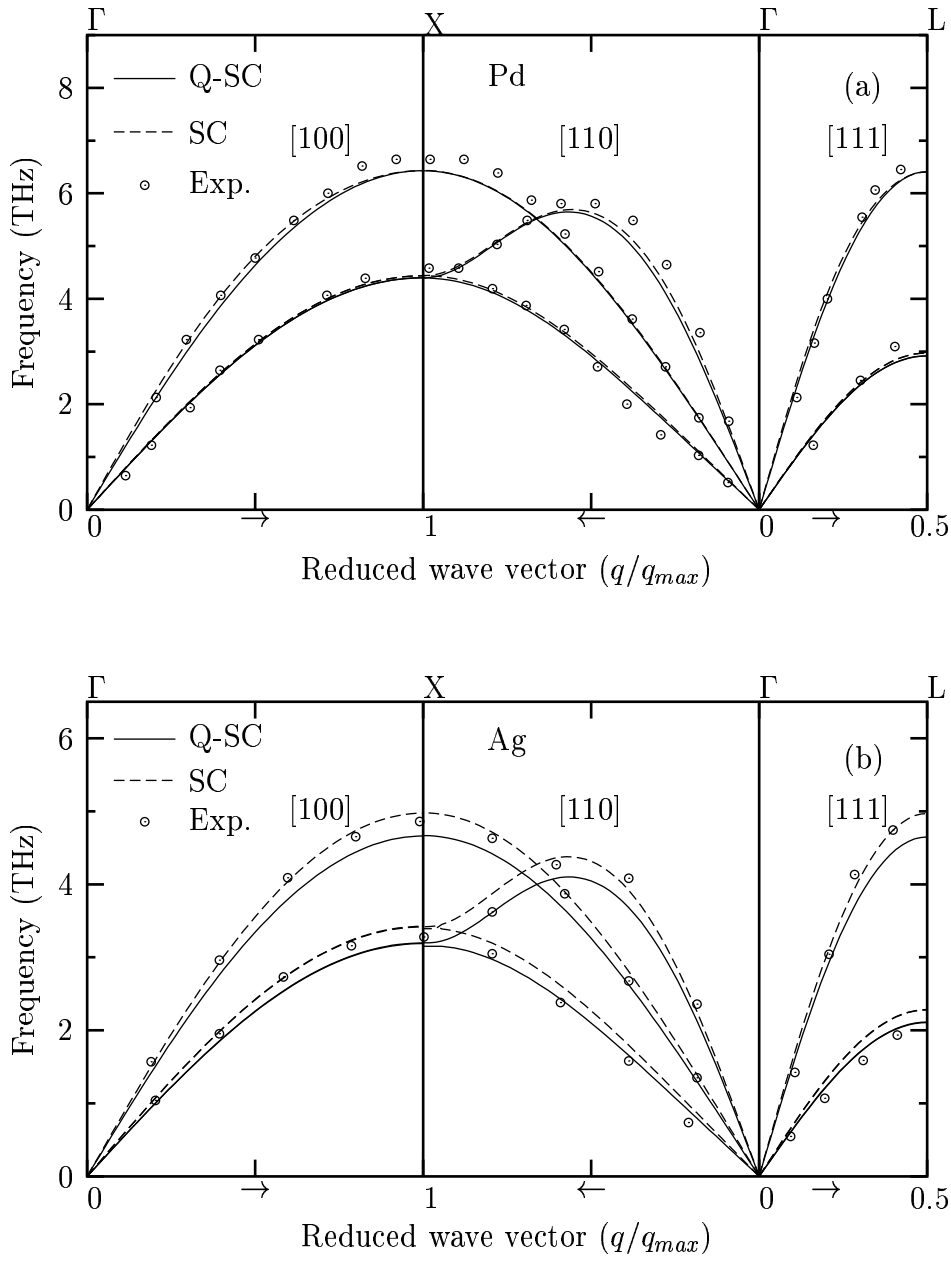
Figure 4.5: Phonon dispersion curves of (a) Pd at 120 K and (b) Ag at 300 K for Q-SC and SC potential parameters along symmetry directions. The circles are experimental data for Pd [125] and Ag [126]. The solid curves give the calculations for Q-SC parameters. The dashed curves represent the SC calculations.
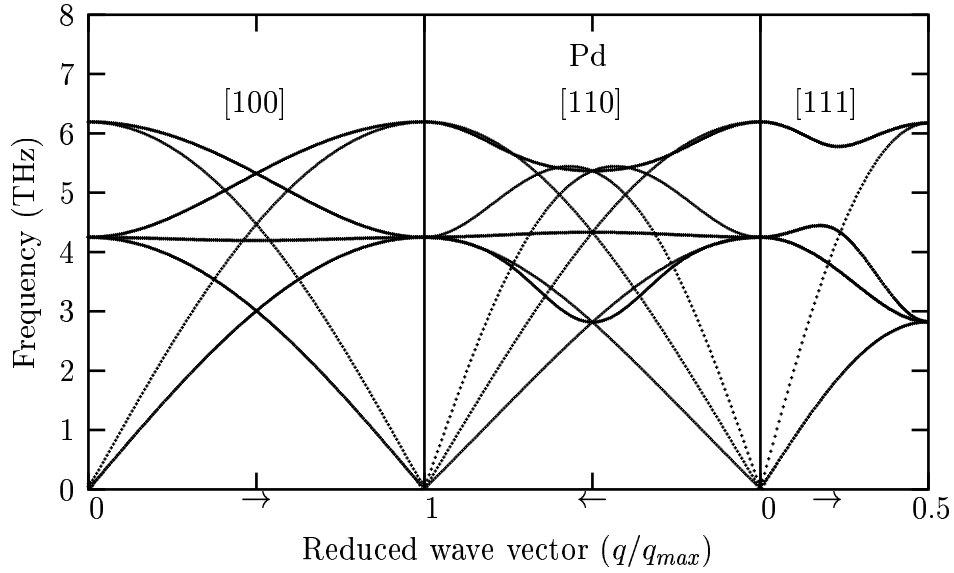
Figure 4.6: Optic and acoustic phonon dispersion curves of Pd at 0.1 K for Q-SC potential parameters.

potential has been fitted only to three experimental quantities and it still is in good agreement with the experimental data.

The behavior of the optical and acoustic phonon dispersion relation for Pd metal is shown in Fig. 4.6. The frequencies of optic modes are higher than those of the acoustic modes, as expected.

4.1.4   Melting Region

The enthalpy and the density as a function of temperature for Pd and Ag are given in Figs. 4.7 and 4.8, respectively, in order to calculate their melting
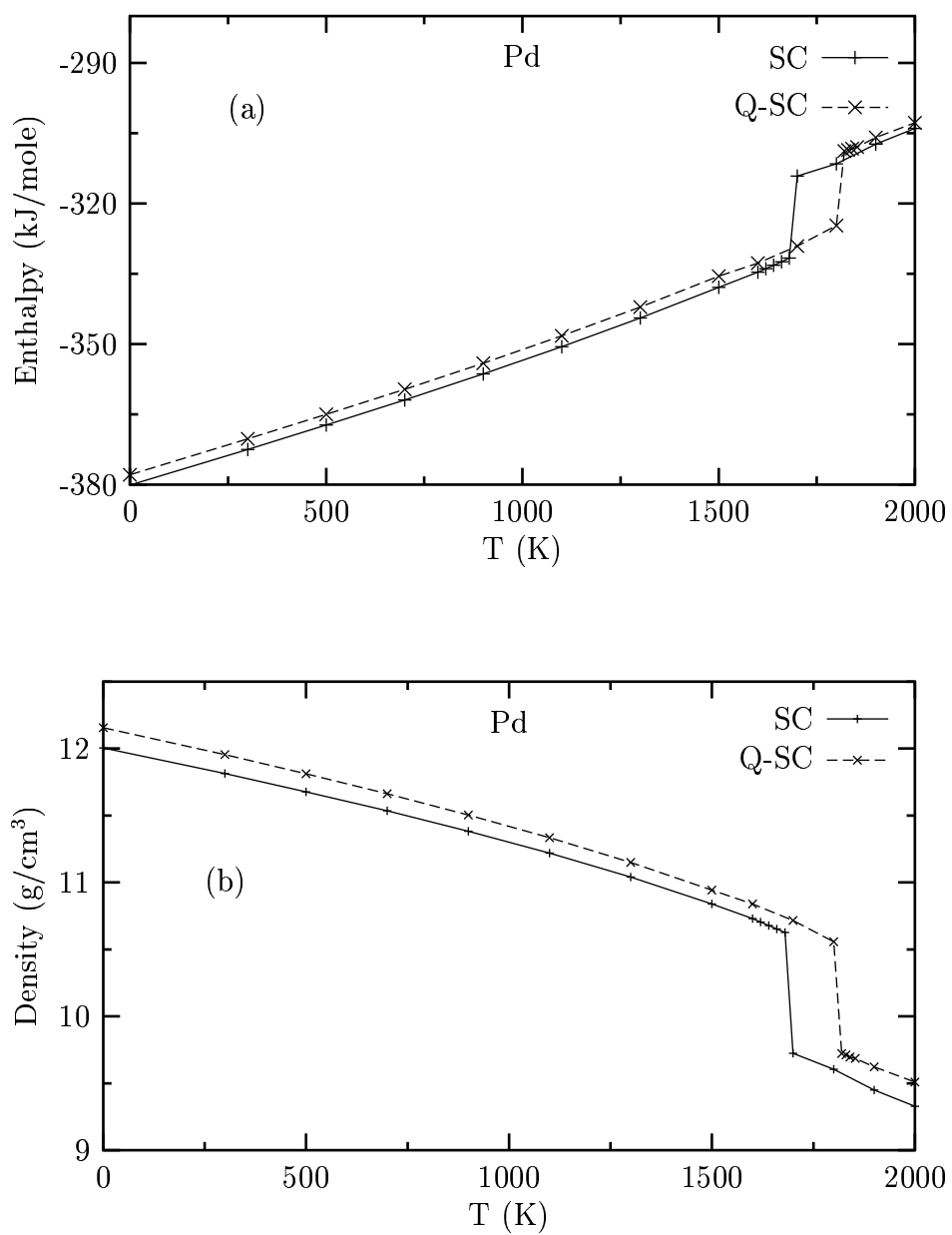
Figure 4.7: (a) Enthalpy and (b) density of Pd calculated by Q-SC and SC potential parameters as a function of temperature.
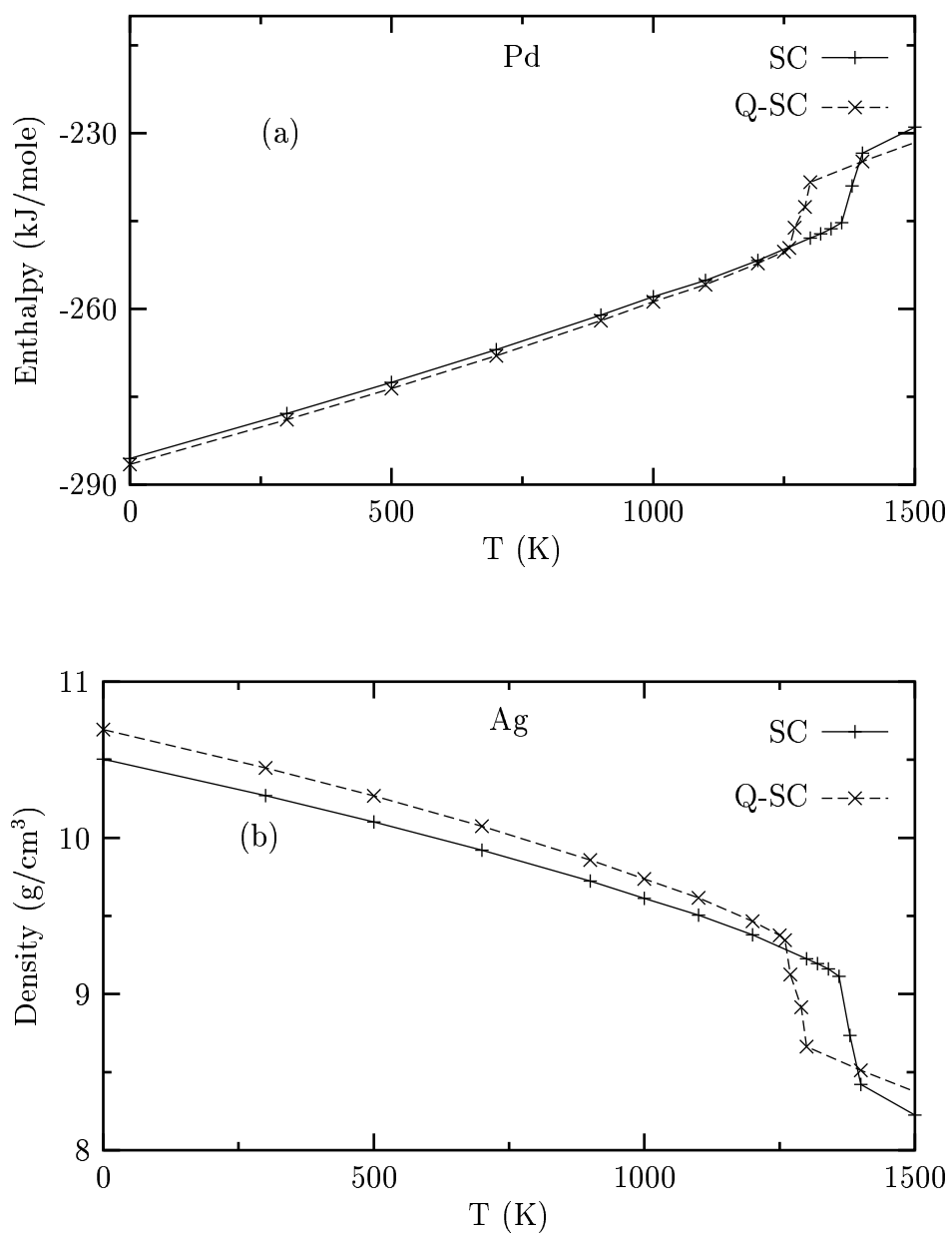
Figure 4.8: (a) Enthalpy and (b) density of Ag calculated by Q-SC and SC potential parameters as a function of temperature.

temperatures. As shown in the graphs, there are sharp jumps in the enthalpy and density. This jump is due to a phase transformation of the material, i.e., material melts at this point. The sharp jumps in the enthalpy and the density graphs indicate the same temperature. We have also considered other physical properties such as volume, pair distribution function, and diffusion coefficient in the prediction of melting point of the material. If we examine the pair distribution function, the peaks after the second disappear. Especially, diffusion coefficient, which is analyzed in detail in the next section, is one of the characteristic properties of liquids. It distinguishes the liquid from the solid. Computer simulations are carried out by 10 K increment to calculate the melting points better, around the melting points of pure metals and alloys. In this manner, the melting points of Pd, Ag and their binary metal alloys are evaluated at different concentrations. We have shown that all physical properties considered here indicate approximately the same melting point of Pd-Ag alloy. The melting points of Pd and Ag obtained by using the Q-SC potential parameters are very close to the experimental data. Therefore, the melting points for the alloy case are evaluated only for Q-SC potential parameters. The melting points of the Pd-Ag system are given in Table 4.3, with available experimental and theoretical data. The evaluated melting points and the experimental ones agree very well. Melting points of Pd and Ag metals are closer to the experimental data rather than other theoretical calculations [117, 127, 128, 129]. The consistency between the simulation results and experimental data for the melting points of Pd, Ag

Table 4.3: The melting points of Pd, Ag and Pd-Ag alloys calculated from SC and Q-SC potentials with the experimental data from Ref. [115] and other theoretical calculations.

	Simulation (K)	Experiment (K)	Other Calculations (K)
Pd	1690±20(SC), 1820±10(Q-SC)	1825	1390[a], 1215[b]
$Pd_{0.8}Ag_{0.2}$	1695±10(Q-SC)	1704	
$Pd_{0.6}Ag_{0.4}$	1570±10(Q-SC)	1620	
$Pd_{0.4}Ag_{0.6}$	1480±10(Q-SC)	1507	
$Pd_{0.2}Ag_{0.8}$	1380±10(Q-SC)	1340	
Ag	1370±20(SC), 1270±10(Q-SC)	1234.9	1170[a], 907[b], 1330[c], 1465[d]

[a] Ref. [129]
[b] Ref. [128]
[c] Ref. [117]
[d] Ref. [127]

and their alloys shows the excellent transferability of the Q-SC potential to high temperature applications.

4.1.5   Pair distribution function

Pair distribution function is of central importance to the modern theory of solids and liquids. The structures and properties of solids and liquids in equilibrium are best described by this function. Pair distribution function may be defined as follows: $g(r)$ is proportional to the probability of finding another atom, at the same instant, at a distance r from the reference atom located at the origin. In this respect, the function $4\pi r^2 n_0 g(r)$ is generally called the radial distribution function (r.d.f.), (where n_0 is the average number density given by N/V). In a binary alloy of components 1 and 2, three pair distribution functions, i.e. the partial distribution functions $g_{11}(r), g_{12}(r), g_{22}(r)$, are required for a complete description of its structure. This function can be extracted from x-ray and neutron diffraction experiments [130]. The pair distribution function $g(r)$ can be
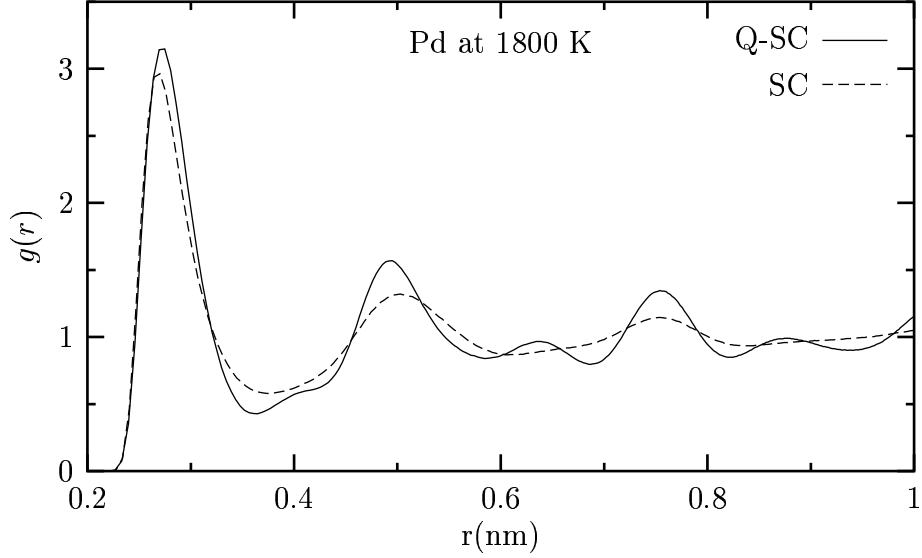
Figure 4.9: Pair distribution function $g(r)$ of Pd at 1800 K calculated by Q-SC and SC potential.

readily computed from trajectories of the atoms [73], since molecular dynamics simulation technique provides positions of individual atoms as a function of time. Pair distribution function has sharp peaks in the solid phase. The peaks of pair distribution function of Pd-Ag alloy decrease at temperatures near to the melting points and shows an oscillation about 1. Figs. 4.9 and 4.10 display the pair distribution function calculated from Q-SC and SC potential parameters to show the structural behavior of Pd at 1800 K and Ag metals at 1300 K, respectively.

SC potential gives rise to liquid state while pair distribution function of Q-SC for Pd is still in the solid phase as shown explicitly in Fig. 4.9. On the other
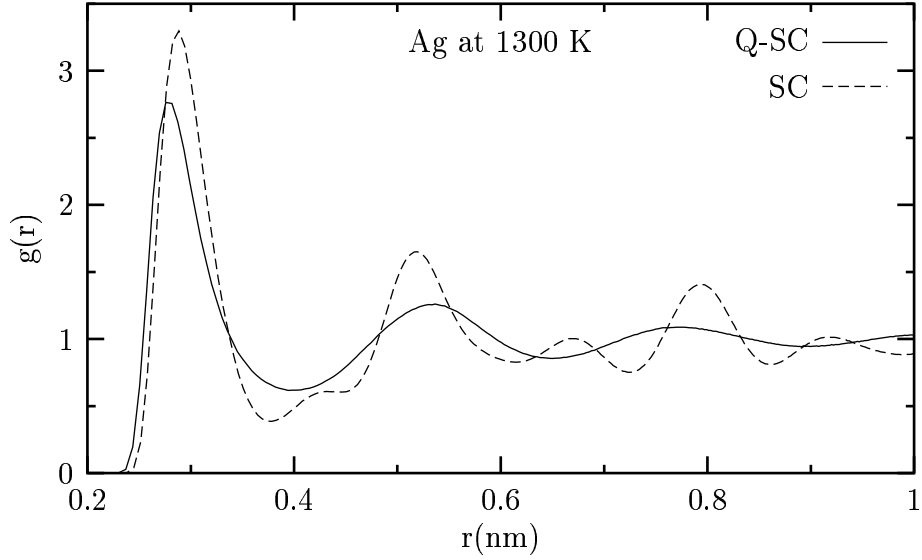
Figure 4.10: Pair distribution function $g(r)$ of Ag at 1300 K calculated by Q-SC and SC potential.

hand, the result for Q-SC is in the liquid phase, but, that for SC is also still in the solid case for Ag metal. The comparisons of $g(r)$ obtained from Q-SC and SC potentials for Pd at 1853 K and Ag at 1273 K with available experimental data is given in Fig. 4.11. Distribution functions calculated from Q-SC potential parameters are in good agreement with the experimental data as seen from both of the figures. Q-SC shows a slight improvement over SC for Ag. Moreover, there is also an improvement in the first peak of Pd.
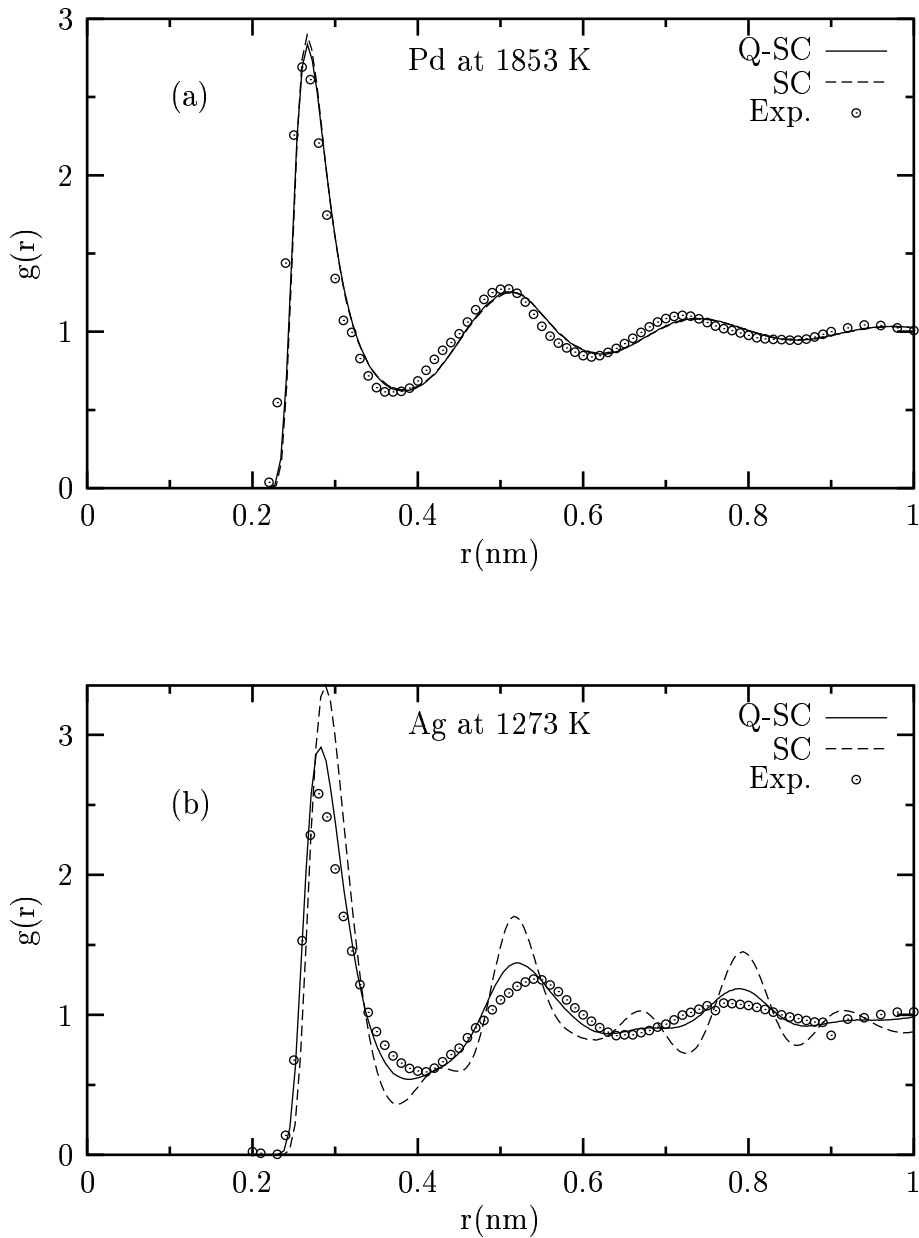
Figure 4.11: a) Pair distribution function $g(r)$ of Pd at 1853 K for Q-SC and SC potential with the experimental data from Ref. [131]. Both potentials show similar behavior at this temperature. b) Pair distribution function $g(r)$ of Ag at 1273 K for Q-SC and SC potential with the experimental data from Ref. [131]. Note that the structure is solidus form for SC potential at the same temperature, thus, indicating the system has still not melted. However the system must be heated up to 1373 K to be melted by SC potential.

4.2 LIQUID PROPERTIES

4.2.1 Introduction

Many solid materials, e.g. glass and crystalline, originate from their liquid states. Their microstructures are little known, and the essential and internal relationship between liquids and solids is still obscure. Therefore, it is indispensable basic physical properties as well as one of the most sensitive physical properties indirectly affecting the information of the liquid structure in discussing the nature and behavior of liquid metals and alloys. From the practical point of view, the viscosity and diffusion coefficient are important parameters in the casting process. However, these quantities for metals and metallic alloys are lacking, because of the difficulties in their measurement. The use of molecular dynamics simulation has been successful for investigating the transport properties of liquid metals.

We present the liquid properties of Pd-Ag system in this section. The transferability of potential parameters from solid to liquid and from elemental case to alloy case are checked by analyzing liquid properties of Pd-Ag system.

4.2.2 Liquid Structure

We present the pair distribution function of Pd and Ag pure metals calculated for both potential parameter sets at the specific temperature in Fig. 4.12 in order to compare with the experimental data and show that Q-SC potential parameter set results are in better agreement with the experimental data than SC potential parameters. The melting points of Pd and Ag are found as 1820 K and 1270

K, respectively, for Q-SC, 1690 K and 1390 K, respectively, for SC. The Q-SC potential parameters for Pd and Ag yield melting points closer to the experimental values which are 1825 K for Pd and 1235 K for Ag, as discussed in section 4.1.4. The pair distribution functions of Pd at 1853 K and Ag at 1453 K are given in Fig. 4.12 with the available experimental data. There is an improvement in the height of the first peak of the pair distribution function of Ag computed from Q-SC potential over SC calculations, as shown in the figure.

4.2.3   Dynamical Properties

4.2.3.1   Diffusion Coefficient

The Einstein relation at the long time limit is given as [75];

$$< |r(t) - r(0)|^2 >= 6Dt + C \qquad , \tag{4.12}$$

where $< |r(t) - r(0)|^2 >$ is the mean square displacement, and D, C are constants. The constant D defines the diffusion coefficient. Mean square displacements as a function of time calculated from Q-SC and SC potential sets for Pd and Ag pure metals are plotted in Figs. 4.13 and 4.14, respectively. Pd is in the liquid state for both potential parameter sets at 1853 K and slope of the SC is slightly greater than that of the Q-SC. The slopes of these lines give the diffusion coefficients at the long time limit. SC gives a very small slope, while Q-SC yields a large slope of the mean square displacement for Ag. The figures show a quadratic dependence at short times. This behavior can be understood immediately by

56
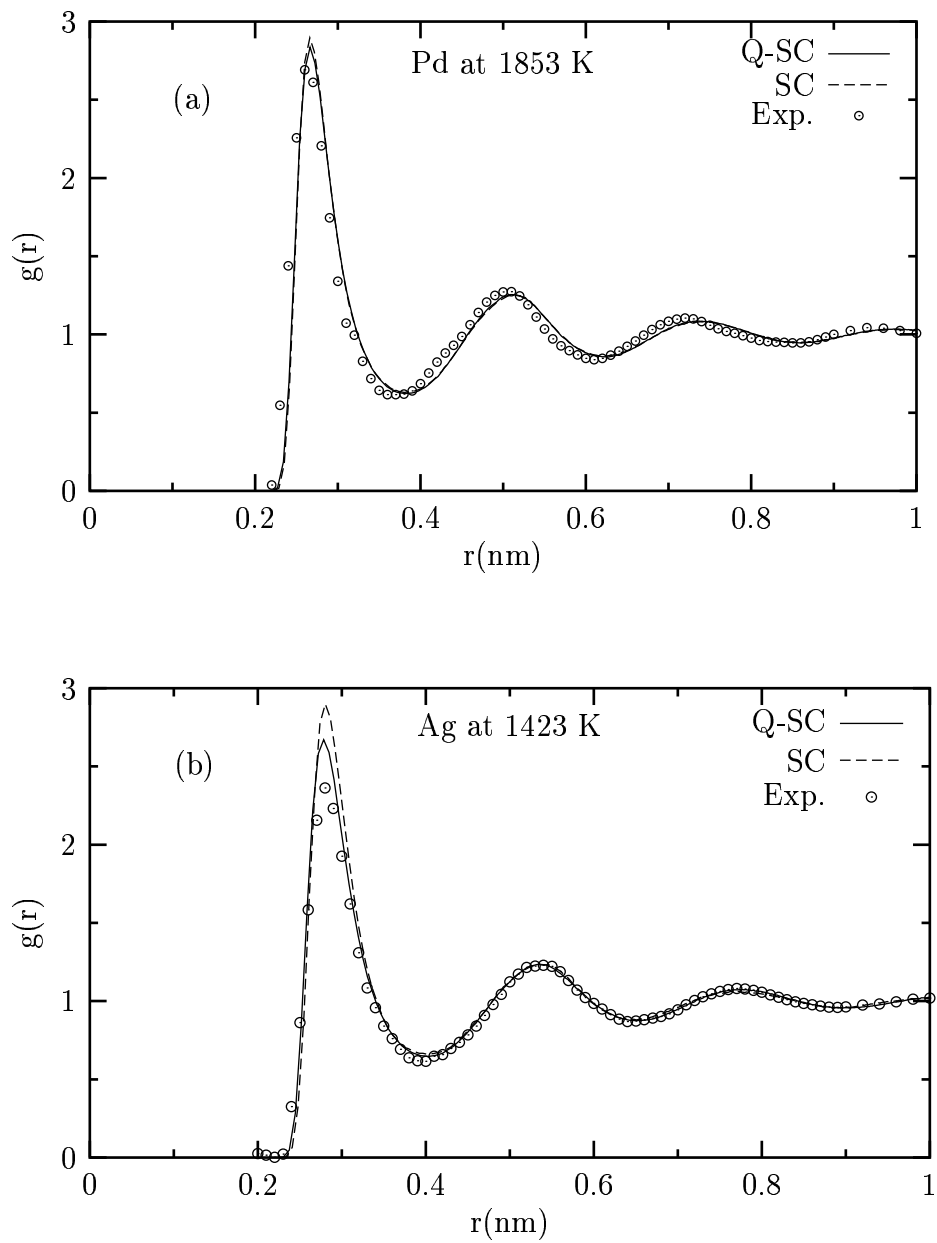
Figure 4.12: Pair distribution function of (a) Pd at 1853 K and (b) Ag at 1423 K for Q-SC and SC potentials with experimental data [131].
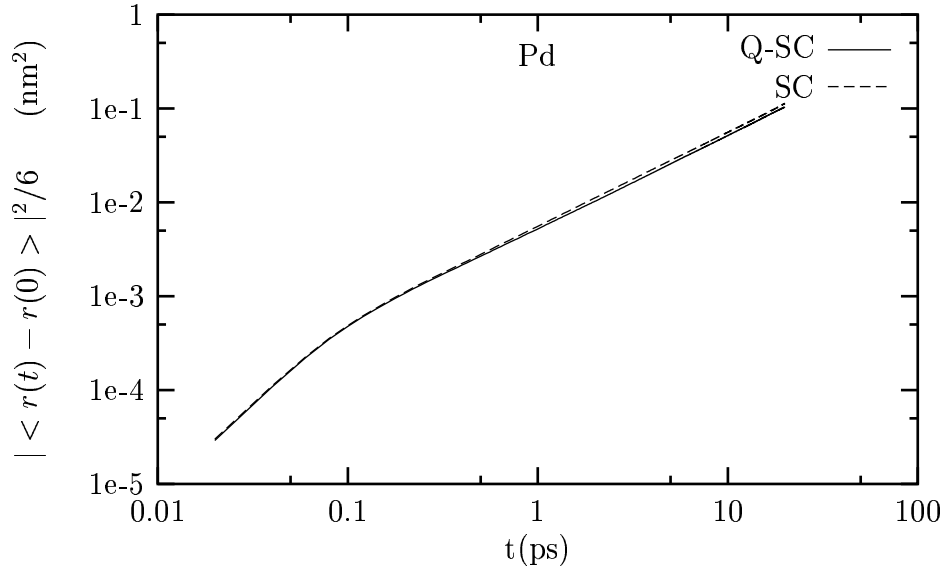
Figure 4.13: The time dependence of the mean square displacement of Pd at 1853 K for the Q-SC and SC potentials in the logarithmic plot. The unit of the mean square displacement is nm^2

realizing that the particles move ballistically at short times. This is due to the cage effect created by the nearest neighbor atoms. The microscopic reason for the presence of plateau is that the tagged particle is trapped in the cage and it takes the particle a long time to escape from this cage. The cages become more and more rigid with decreasing temperature, and thus the time needed to break them up increases. The particles start to collide with their neighbors and their motion becomes diffusive for longer times.

Diffusion coefficient D may also be calculated from velocity auto-correlation function via the Green-Kubo relation [75];
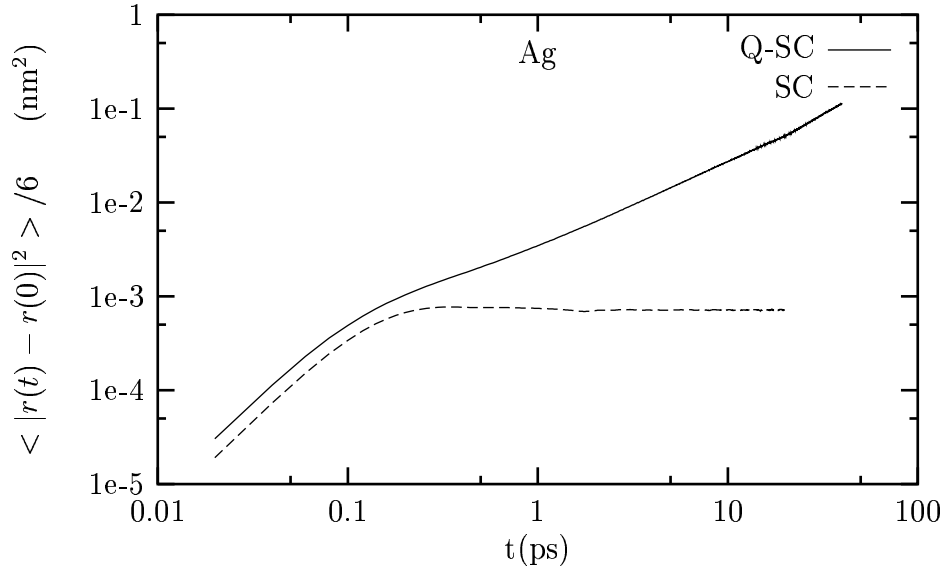
Figure 4.14: The time dependence of the mean square displacement of Ag at 1273 K for the Q-SC and SC potentials in the logarithmic plot.

$$D = \frac{1}{3} \int_0^\infty dt < v_i(t).v_i(0) > \qquad . \qquad (4.13)$$

where $v_i(t)$ is the center of mass velocity of a single molecule. Normalized velocity auto-correlation function $C(t)$ is given as [73];

$$C(t) = \frac{< v_i(t).v_i(0) >}{< v_i(0).v_i(0) >} \qquad . \qquad (4.14)$$

This normalized function gives that values of velocity at two times separated by a period of time t are related and it highlights the statistical nature of the correlation function. When $C(t)= 1$, as at t $= 0$, there is a complete correlation of values

59

with a 100 percent certainty. When $C(t) = 0$, as it may often do when t is large, there is no relationship between any two values over this particular time interval. Normalized velocity auto-correlation function (VACF) for Ag at 1273 K computed from both Q-SC and SC potentials to compare the results obtained from both potential sets is given in Fig. 4.15. The same function for Ag in $Pd_{0.6}Ag_{0.4}$ alloy calculated for only Q-SC at different temperatures to comprehend diffusion processes in the solid and liquid states, is given in Fig. 4.16, respectively. $C(t)$ remains positive for all times and decay monotonically to zero at high temperatures, but this function becomes negative and passes through a minimum before approaching zero at low temperatures, as seen in Fig. 4.16. The negative correlation region interpreted as a rebound of the tagged particle against the cage formed by its nearest neighbors take place up to high temperatures far away from the melting points. Collisions tend to scatter without reversing their trajectories at high temperature. Hence, $C(t)$ remains positive. However, rebounding collisions are more numerous than scattering collisions at low temperature in the solid case, and many rebounds cause $C(t)$ to change sign.

Diffusivities in solid state differ from those in liquid state by a factor of 100 to 1000 in the case of metals. The high atomic mobility of most metals just above their melting temperature, with the diffusivities of the order of $10^{-3}nm^2ps^{-1}$, is one of the most characteristic properties of liquids [130]. The diffusion coefficients calculated from Eqs. 4.12 and 4.13 for the potential sets considered in this study at the specific temperatures for Pd and Ag metals in the constant temperature

60
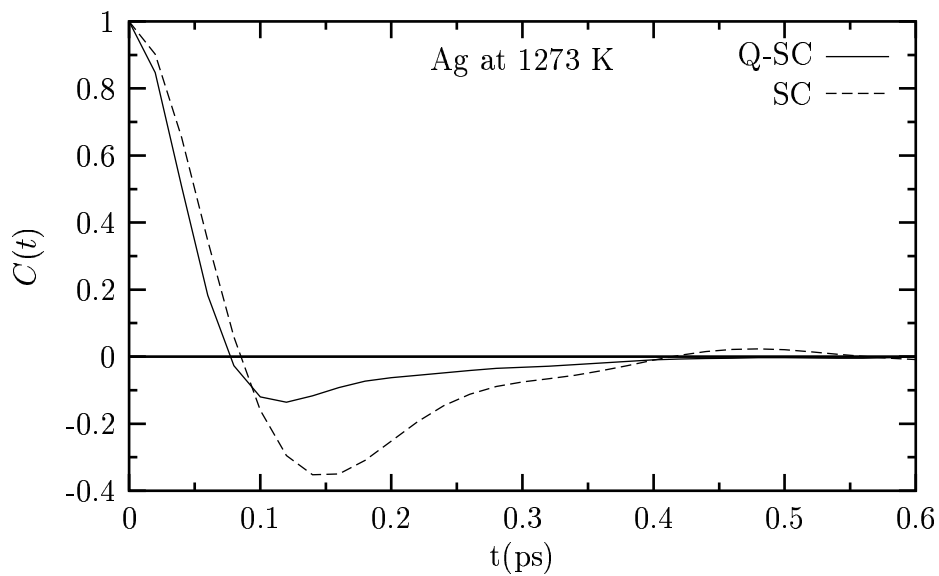
Figure 4.15: Normalized velocity auto-correlation function of Ag at 1273 K for the Q-SC and SC potentials.
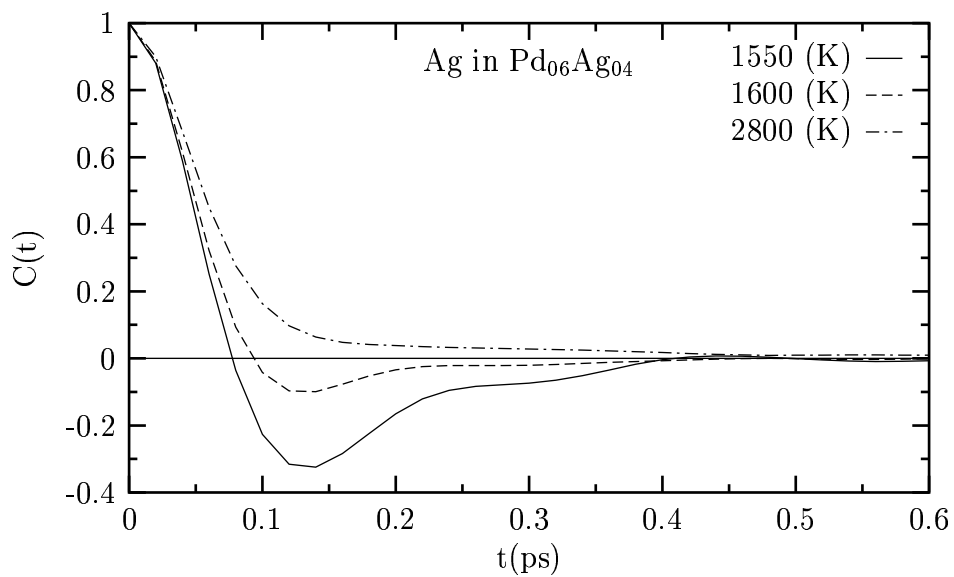
Figure 4.16: Normalized velocity auto-correlation function of Ag in $Pd_{0.6}Ag_{0.4}$ at different temperatures for the Q-SC potentials.

and pressure (TPN) and microcanonical (EVN) ensembles are given in Table 4.4, with the available experimental and theoretical data. The diffusion coefficients computed from Q-SC parameter set produce more accurate values. The values are compatible with both experimental data [132] and other theoretical calculations [133, 134].

Table 4.4: Values of the diffusion coefficients D in the units of nm^2/ns. Pd and Ag liquid metals are computed by using Green-Kubo (GK) and Einstein (E) relations at the specific temperatures in the two different ensembles (TPN and EVN) for two different potential parameter sets (Q-SC and SC). The diffusion coefficients in the EVN ensemble are calculated from the fitting to the Arrhenius equation.

	T (K)		D in TPN		Fitted D in EVN		Exp.
			GK	E	GK	E	
Ag	1273	Q-SC	3.43	2.77	3.37	3.43	
		SC	-	0.041			
							2.81[a]
			2.65[b]	2.70[b]			
			2.60[c]	2.65[c]			
Pd	1853	Q-SC	4.87	5.19	4.66	4.69	-
		SC	5.33	5.59			
			4.03[b]	4.07[b]			
			3.80[c]	3.83[c]			

[a]Ref. [132]
[b]Ref. [134]
[c]Ref. [133]

The temperature dependence of the self-diffusivity $D(T)$ is of special interest since the diffusional activation energy is experimentally accessible. It can be computed by fitting the diffusion coefficients calculated by both Einstein and Green-Kubo relations to the Arrhenius form. The formula used in the analysis for the diffusion of liquid metals is Arrhenius type given as [135];

$$D(T) = D_0 exp(-E_a/k_B T) \qquad . \qquad\qquad (4.15)$$

where E_a is the diffusional activation energy, k_B is Boltzman constant, and T is the absolute temperature. Temperature dependence of self-diffusion coefficient of Pd and Ag in the $Pd_{0.6}Ag_{0.4}$ alloy evaluated from Einstein relation is given in Fig. 4.17, with the Arrhenius fit. The data in the figure fit well to the Arrhenius form. We could not compare our results with the experimental and theoretical data because of their nonexistence in the literature. However, the diffusion coefficients from two methods are mutually consistent with each other. Self-diffusion coefficients of Pd-Ag alloys are computed by using Q-SC potential parameters to study the effect of the concentration on the diffusion coefficients. The results obtained from Einstein relation are fitted to Arrhenius equation and are collected in Table 4.5. Arrhenius fitting parameters are also included in the same table. Diffusion of Ag is larger than that of Pd at the specific temperature as can be seen in Table 4.5. The self-diffusion coefficients for Pd-Ag system increase, as to be expected, while the concentration of Ag in Pd increases. Our results may be tested by experimental and first-principle calculations.

4.2.3.2 Viscosity

Another important physical property of liquid metals is the shear viscosity. It may be calculated from Green-Kubo relationship by integrating the shear stress auto-correlation function. The shear viscosity is given as follows [75];
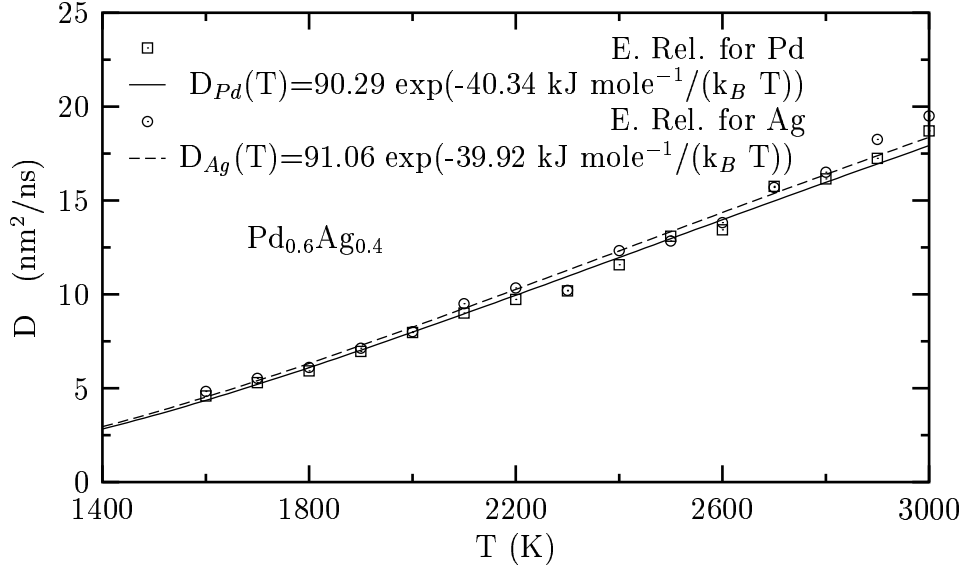
Figure 4.17: Self-diffusion coefficients D of Pd and Ag in $Pd_{0.6}Ag_{0.4}$ alloy calculated from Einstein relation (E) as a function of temperature with the Arrhenius fit by using Q-SC potential.

$$\eta = \frac{V}{k_B T} \int_0^\infty dt < \mathcal{P}_{\alpha\beta}(t).\mathcal{P}_{\alpha\beta}(0) > \qquad , \qquad (4.16)$$

where $\mathcal{P}_{\alpha\beta}$ is an off-diagonal ($\alpha \neq \beta$) element of the shear tensor. The shear viscosities fitted to Arrhenius expression $\eta = \eta_0 exp(E_a/k_B T)$ for $Pd_{0.6}Ni_{0.4}$ are given in Fig. 4.18. The values of viscosity for the alloy decreases exponentially by obeying the Arrhenius form as the temperature increases. Furthermore, the effects of the concentration on the viscosity computed from Green-Kubo formulae over 50000 steps in the microcanonical ensembles (EVN) are also investigated at the temperature of 2000 K. Table 4.6 lists the viscosities fitted to Arrhenius

Table 4.5: Arrhenius fitting parameters (D_0 and E_a) and self-diffusion coefficients (D) as evaluated by using the Einstein relation for Pd-Ag alloys at 2000 K. Here the computed diffusion coefficients are obtained from Arrhenius equation. D, D_0 and E_a are in the units of nm^2/ns and kJ/mole, respectively

	Pd		Ag		Pd	Ag
	D_0	E_a	D_0	E_a	D	D
Pd	103.00	47.60	-	-	5.88	-
$Pd_{0.8}Ag_{0.2}$	107.05	45.49	111.52	45.99	6.94	7.02
$Pd_{0.6}Ag_{0.4}$	90.29	40.33	91.06	39.93	7.99	8.25
$Pd_{0.4}Ag_{0.6}$	99.89	39.71	99.73	39.26	9.17	9.41
$Pd_{0.2}Ag_{0.8}$	122.36	41.70	131.88	42.51	9.97	10.23
Ag	-	-	102.31	36.11	-	11.63

equation for Pd-Ag alloys. The values of viscosity decrease while increasing the concentration of Pd in Ag, as seen in the table. This trend is expected result of this material. Arrhenius fitting parameters are also given in the same table to calculate the viscosity at the desired temperature and the specific concentration. Table 4.6 includes also viscosity values for pure Pd and Ag at the specific temperature of 1853 K and 1273 K to compare together with available experimental data [136] and other calculations [133, 134, 137]. There is an available experimental data for only Ag metal for Pd-Ag system . The results for viscosity are smaller than those of available experimental value and other calculations. This discrepancy for viscosity can be improved by trying the non-equilibrium molecular dynamics (NEMD) technique.
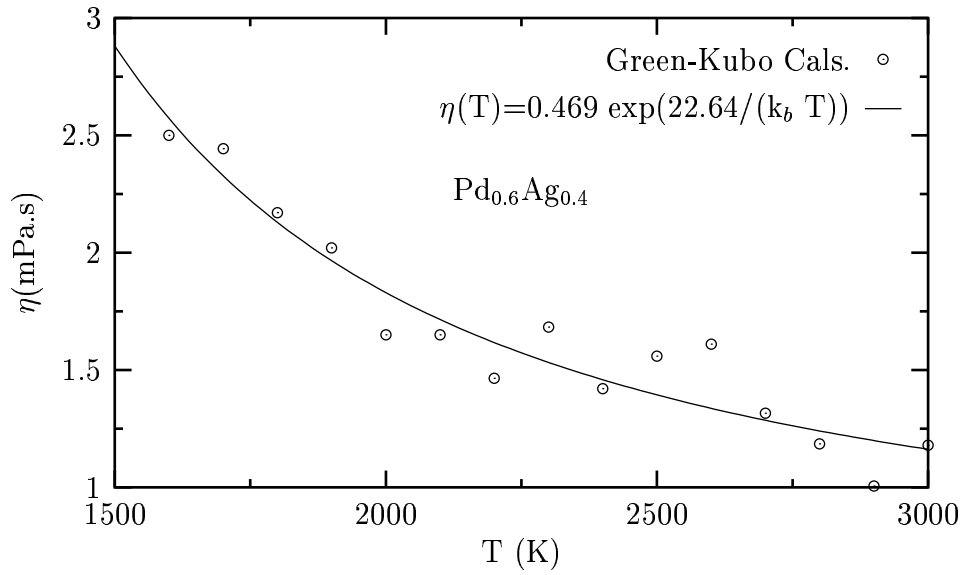
Figure 4.18: Viscosity values of the $Pd_{0.6}Ag_{0.4}$ alloy calculated from Green-Kubo relation as a function of temperature alloy along with Arrhenius fit for Q-SC potential parameters.

Table 4.6: Arrhenius fitting parameters (η_0 and E_{vis}) and shear viscosity (η) values evaluated by using the Green-Kubo (GK) relation for Pd-Ag alloys at 2000 K. Here the shear viscosity is obtained from Arrhenius equation.

| | η_0 (mPa.s) | E_{vis} (kJ/mole) | T(K) | η(mPa.s) | | |
				Sim.	Exp.	Other Cal.
Pd	0.479	27.82	2000	2.55		
			1853	2.91	-	4.00^b, 3.68^c
$Pd_{0.8}Ag_{0.2}$	0.392	28.64	2000	2.19		
$Pd_{0.6}Ag_{0.4}$	0.469	22.64	2000	1.83		
$Pd_{0.4}Ag_{0.6}$	0.446	21.39	2000	1.61		
$Pd_{0.2}Ag_{0.8}$	0.291	26.67	2000	1.45		
Ag	0.395	17.98	2000	1.17		
			1273	2.16	3.88^a	3.84^b, 3.68^c
						3.38^d

[a]Ref. [136]
[b]Ref. [133]
[c]Ref. [134]
[d]Ref. [137]

4.3 GLASS FORMATION AND CRYSTALLIZATION

4.3.1 Introduction

Solid state amorphization is a well-known structural phase transformation that, evolving from a crystalline state, produces a disordered phase characterized by the lack of long-range order. The liquid metals can be transformed into glasses without long-range order by cooling them rapidly below their freezing temperatures. The structural changes that take place during the cooling processes are small, therefore atomic motion is investigated for an explanation for this transition. There has been much progress in the understanding of the thermodynamic transition of glass [2, 42, 106, 138, 139] in recent years. A glass may be very similar to a frozen liquid. The configurations of the glasses at low temperatures are not far from those of liquid. In fact, glasses can not simply be considered as *frozen liquid*. Understanding the nature of glass formation is an important practical issue. Unlike window panes, metallic glasses are not transparent or brittle, yet their unusual atomic structure gives them distinct mechanical and magnetic properties. They spring more readily back to their original shape after being deformed. The properties of metallic glasses made from liquids depend on the microstructure of materials. The knowledge of microscopic processes of glass transition is essential for understanding and controlling material properties. However, the high cooling rate restricts the practical application of the amorphous techniques. Experiments have not allowed us to directly measure how an atom moves to a particular neighbor in a glass or to observe the motion of a particular

atom in the system. The nature of the glass formation determined by experiment is hardly possible. MD provides the opportunity to directly observe the insight of the glass formation at atomic level.

4.3.2   Glass Formation Tendency and Crystallization

4.3.2.1   Volume and Enthalpy

Figs. 4.19 (a) and (b) represent the variation of volume and enthalpy of $Pd_{0.8}Ag_{0.2}$ as a function of temperature at three different cooling rates, respectively. There is a sharp jump during the heating and cooling processes, as shown in the figures. The sudden increase or decrease is due to the first order transition such as melting and crystallization. The melting temperature of $Pd_{0.8}Ag_{0.2}$ is 1695±10 K which is in reasonable agreement with the experimental melting temperature of 1704 K. Among the reasons for the melting temperature to be a little bit different than the experimental value are that the system is homogeneous without any free surface and we started the simulation with a perfect crystal. The system might not have had time to rearrange an equilibrium distribution of defects. These might cause the melting point to be different from the experimental value. This alloy changes into crystalline form at 0.5 K/ps while it transforms into a glass at faster cooling rates. That is, there is no sudden change in the volume and enthalpy at fast cooling rates. This is a sign of glass formation.
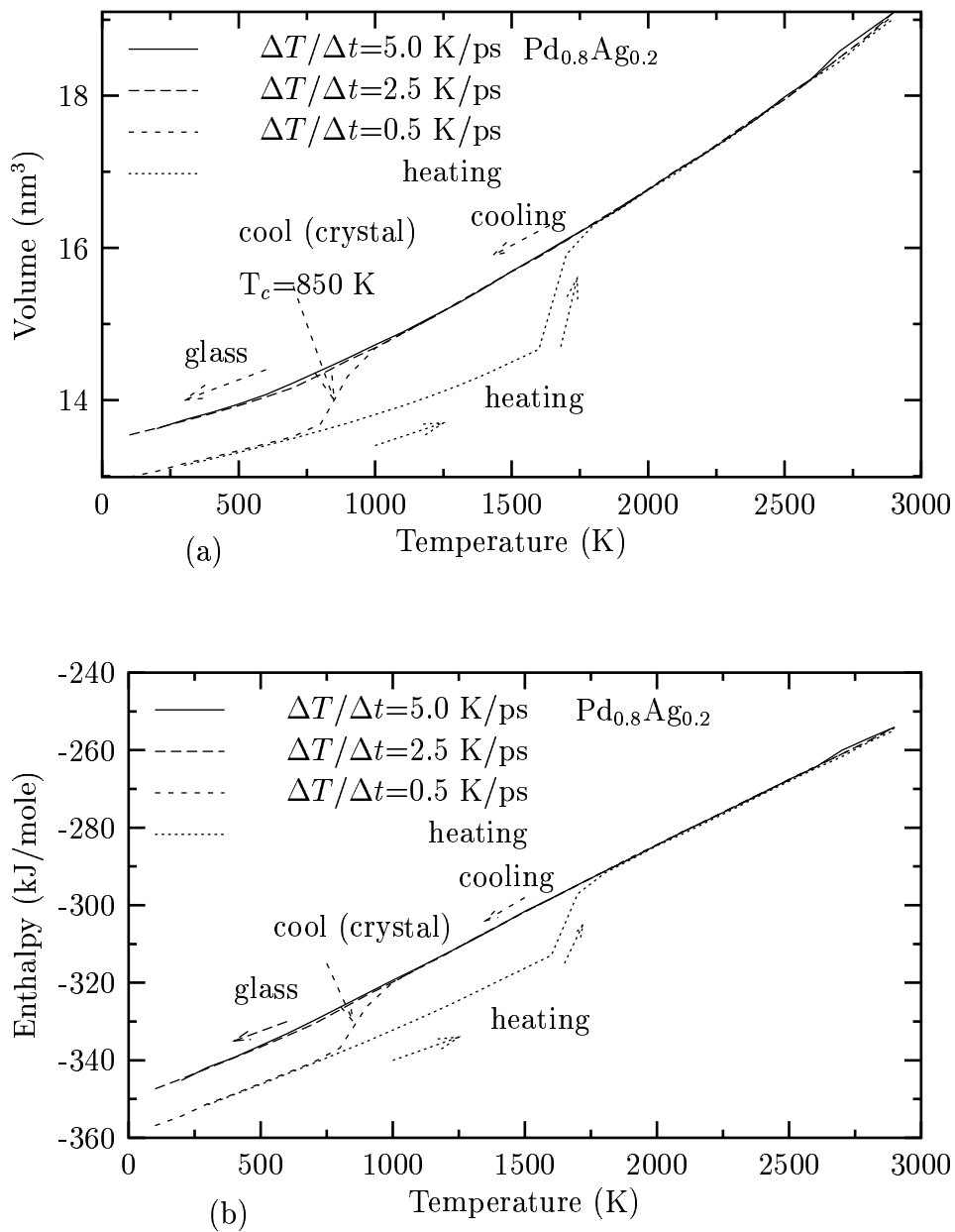
Figure 4.19: a) Volume and b) enthalpy of $Pd_{0.8}Ag_{0.2}$ as a function of temperature during the heating and cooling processes at different cooling rates.

4.3.2.2 Pair Distribution Function

Figs. 4.20 and 4.21 show the pair distribution functions during the heating and cooling processes at three different cooling rates and at different temperatures to investigate the cooling rates effects on the structure of $Pd_{0.8}Ag_{0.2}$. Pair distribution functions represent the sharp peaks during the heating and cooling processes at the rate of 0.5 K/ps. The alloy system recrystallizes and shows the same structure with the heating processes after cooling the model system with the 0.5 K/ps . However, other cooling rates give rise to glass formation of the system. In other words, faster cooling rates lead to glass structure, i.e, there is a splitting in the pair distribution function at 300 K and 700 K, this is a characteristic of metallic glass. Material at 1600 K is still in crystalline form during heating process, but it has supercooled liquid form at three different cooling rates, as shown in Fig. 4.21 (a). The material displays the same structure at all cooling rates at this temperature. The sample is heated from 0 K to 3000 K and cooled by 100 K decrements untill the target temperature of 1800 K is reached in Fig. 4.21 (b). This leads to the same structure at heating and all cooling rates, indicating a stable liquid state.

4.3.2.3 Wendt-Abraham Parameter

Glass and crystallization temperatures can also be predicted by means of the Wendt-Abraham parameter [140], defined by the $R^{WA}(g_{min}/g_{max}) = g_{min}/g_{max}$.
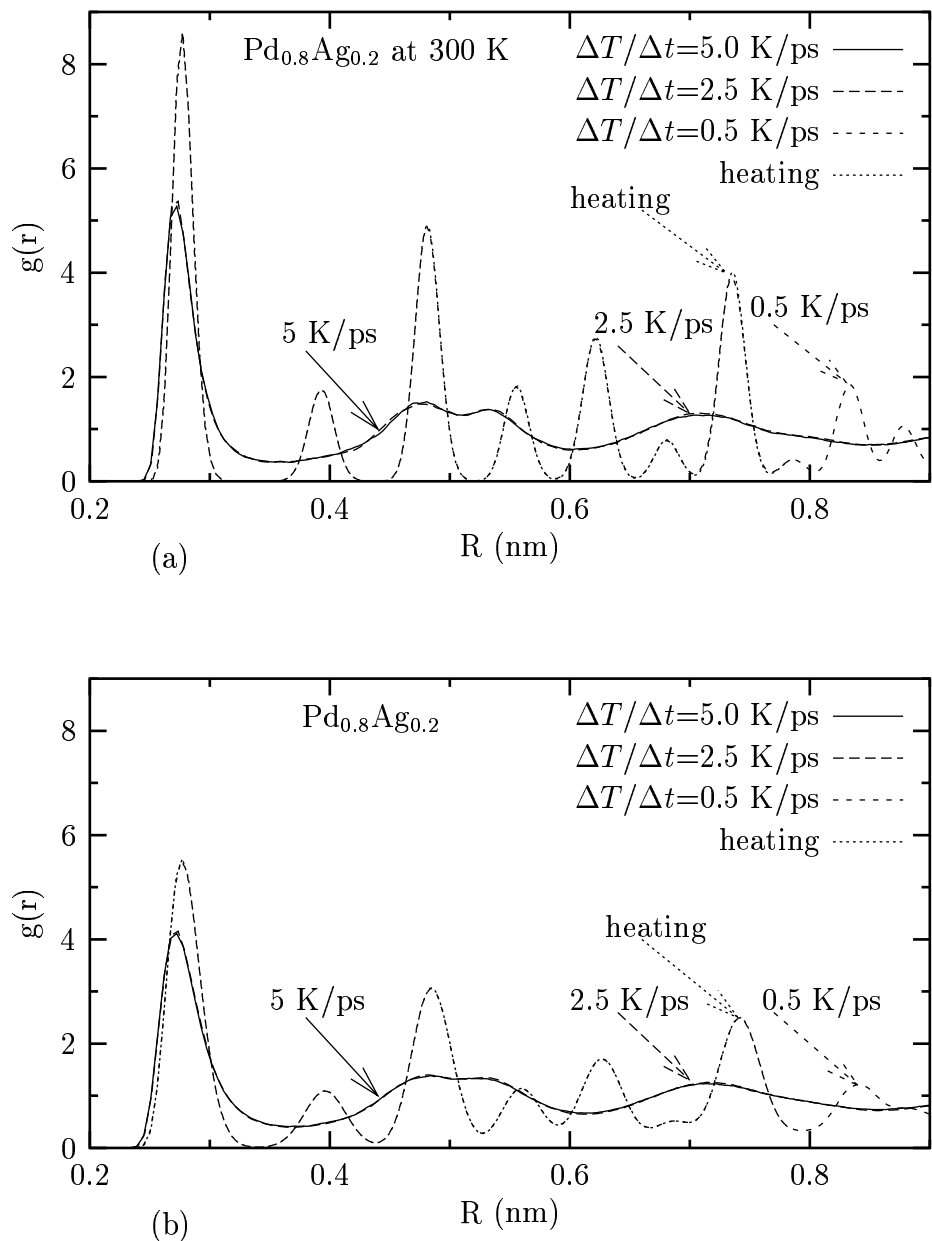
Figure 4.20: Pair distribution functions for structure obtained from heating and cooling cycles at a) 300 K and b) 700 K.
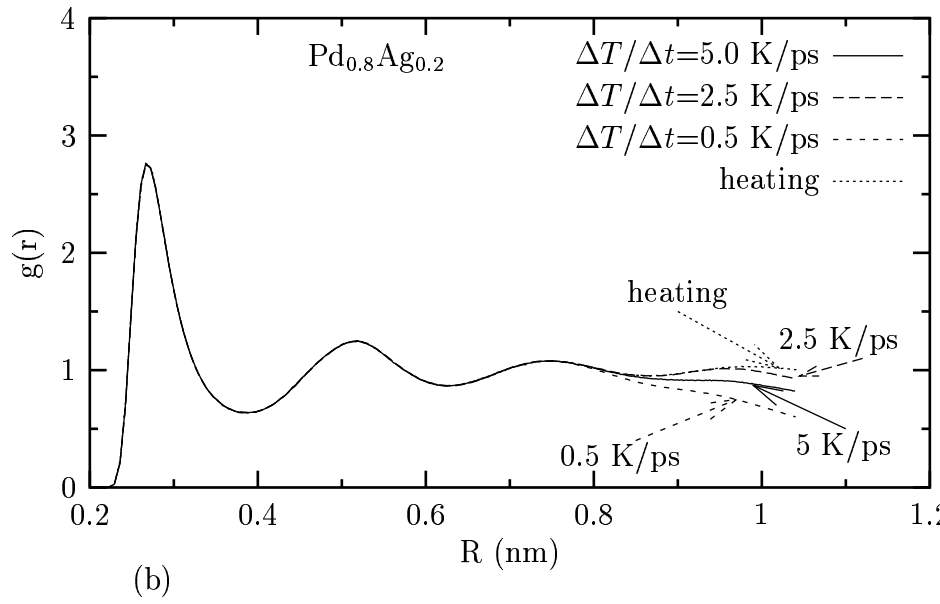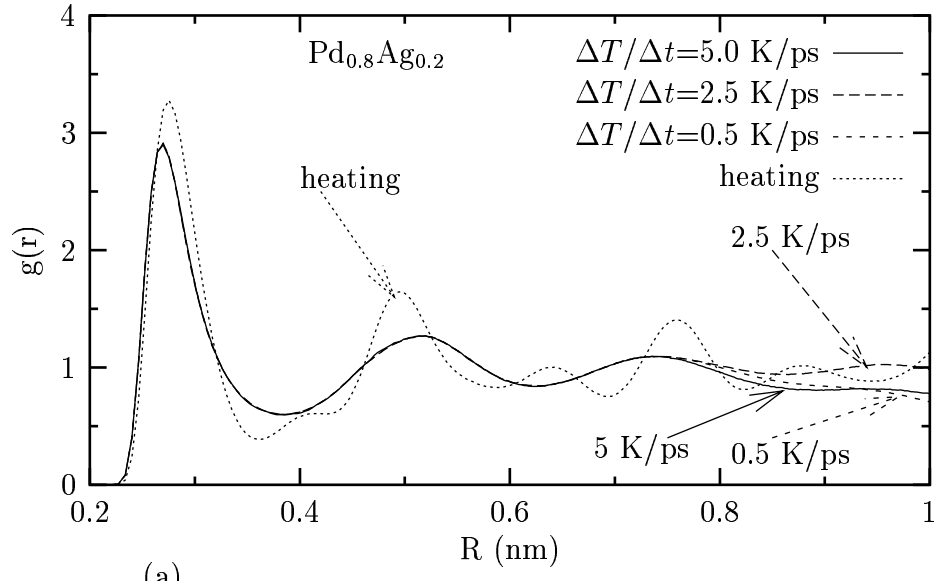
Figure 4.21: Pair distribution functions for structures obtained from heating and cooling cycles at a) 1600 K and b) 1800 K.

The Wendt-Abraham parameter describes the local properties of the pair distribution function which allows one to estimate the glass and crystallization temperatures. The Wendt-Abraham glass and crystallization temperatures are displayed in Fig. 4.22 at different cooling rates. The system shows a glass formation tendency at the temperatures of 400 K and 450 K at the cooling rates of 5.0 K/ps and 2.5 K/ps, respectively, while the slower cooling rate of 0.5 K/ps leads to crystallization at 850 K. The material has not enough time to relax at fast cooling rates. This leads to an amorphous structure, but the material crystallizes as the simulation time increases. Thus, the cooling rates play an important role in determining whether the material change into crystal structure or not.

4.3.2.4   Diffusivity in Metallic Glass Former

Diffusion coefficients of $Pd_{0.8}Ag_{0.2}$ are calculated from the Einstein relation which is given in the Eq. 4.12 and are plotted in Fig. 4.23. Diffusion increases linearly during heating while it decreases exponentially during cooling as a function of temperature, as shown in the figure. The diffusion coefficients for two cooling rates show the same behavior. Diffusion coefficients diminish sharply at the crystallization point. This is an expected result since the system becomes frozen and stays that way within a time scale. The atoms lose their configurational freedom and vibrate around their local positions in the crystalline phase. Our results can not be compared with the experimental data because we lack data for diffusion of Pd and Ag in $Pd_{0.8}Ag_{0.2}$ alloy.
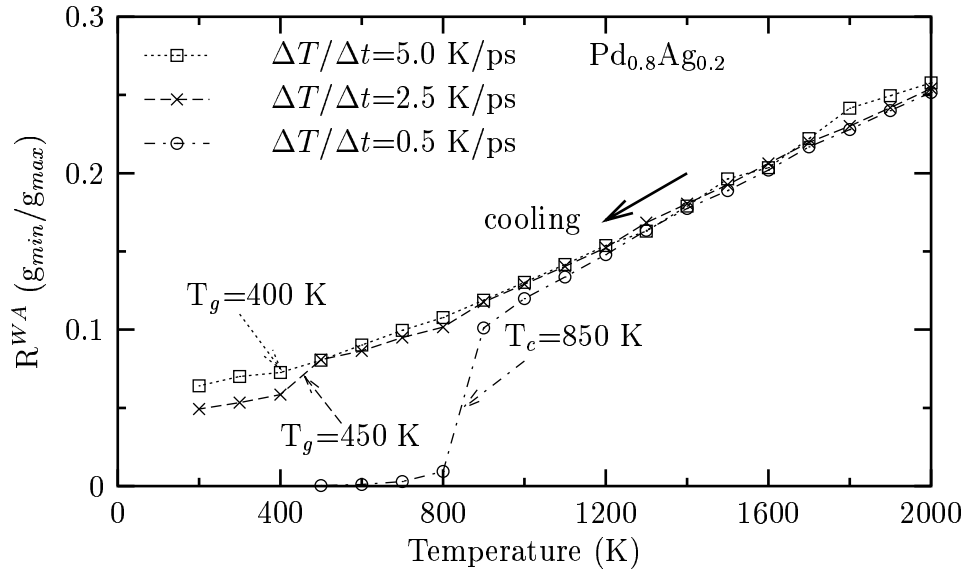
Figure 4.22: Wendt-Abraham parameter R^{WA} versus temperature. 0.5 K/ps leads to crystallization of the material at 850 K. The calculated glass temperatures are 400 K and 450 K at two other cooling rates.

4.3.2.5 The Concentration Effects on the Glass Transition

The concentration effects on the glass transition and crystallization are studied by plotting volume of Pd-Ag alloys as a function of temperature. This graph is given in Fig. 4.24. The increase in concentration of Ag atoms in Pd-Ag alloys leads to amorphous structure at the cooling rate of 0.5 K/ps, as seen in the figure, that is, the material requires more time to rearrange and crystallize. This is due to the Ag atoms being faster in the Pd-Ag alloy than the Pd atoms.
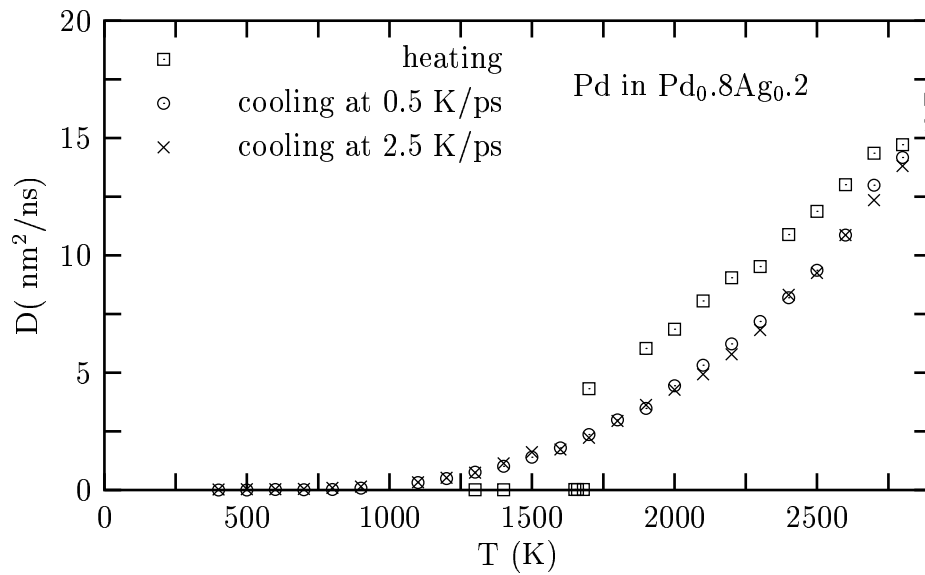
Figure 4.23: Diffusion coefficients versus temperature during heating processes in EVN dynamics and cooling processes in TVN dynamics for Pd in $Pd_{0.8}Ag_{0.2}$ alloy at 2.5 K/ps and 0.5 K/ps cooling rates.
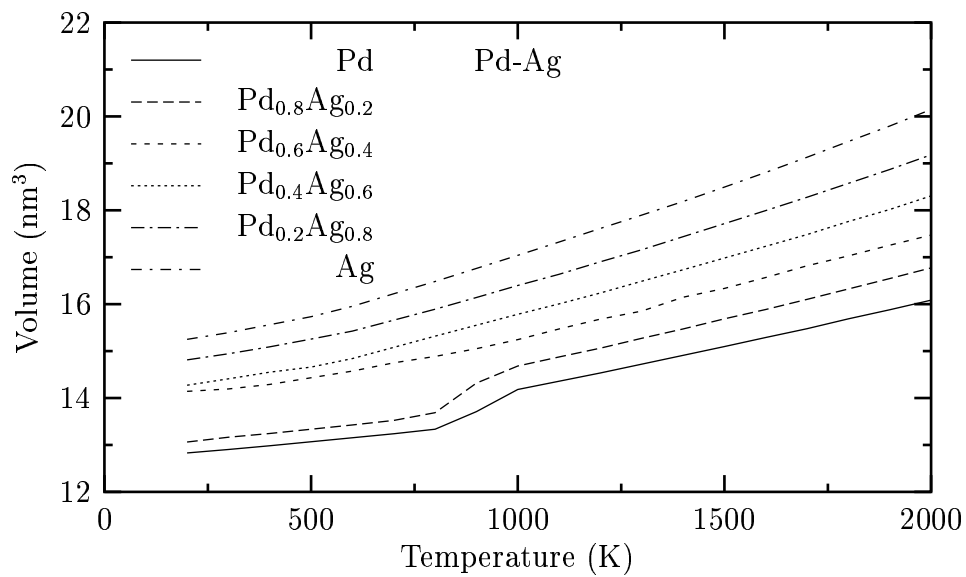
Figure 4.24: Concentration effect on the crystallization and glass formation of Pd-Ag alloys at the cooling rate of 0.5 K/ps.

4.4 INTERMETALLICS

Until now, we have considered only the random alloys. It is of great impor-
tance to also investigate ordered alloys. We have chosen to study the interesting
case of intermetallics.

In this section, computer simulations of Cu, Au pure metals and their ordered
intermetallics alloys, $Cu_3Au(L1_2)$, $CuAu(L1_0)$, and $CuAu_3(L1_2)$, are performed in
three successive ensembles, that is, constant-enthalpy constant-pressure (HPN),
constant-temperature constant-pressure (TPN), and microcanonical (EVN) en-
sembles. The simulation box is made up of 1372 particles arranged on the fcc
structure for the Cu and Au pure metals, $L1_2$ structure for the Cu_3Au and $CuAu_3$,
and $L1_0$ structure for the CuAu ordered intermetallic systems. In the case of
Cu_3Au, the Au atoms occupy the corner cites, while Cu atoms occupy the face
centers of the basis cube; the opposite occurs for $CuAu_3$. In the ordered phase,
CuAu has a tetragonal structure and consists of alternate planes of Cu and Au
atoms. The structure can be thought of as a distorted face-centered cubic lattice,
in which the experimental value of c/a is 0.926.

4.4.1 Thermodynamical Properties

4.4.1.1 Lattice Parameter, Cohesive Energy, and Density

In Table 4.7, we present results of the cohesive energies, the equilibrium lat-
tice constants, and density for the Cu and Au pure metals calculated from TPN
ensemble average over 20000 time steps at various temperatures along with the

available experimental data. The Q-SC calculations of the cohesive energy, lattice parameter and density are in good agreement with the experimental data [116]. Especially, the results of the Q-SC are closer to the experimental data than those of SC as temperature increases. For example, simulation results of the lattice parameter and density for the Q-SC show approximately 0.2 % and 0.8 %, respectively, at temperature of 0 K. For the SC these deviations are 0.3 % and 0.9 %, respectively, at 0 K. But, the deviations for the SC calculation are greater than those of Q-SC. As an additional remark, it can be said that as the temperature increases the deviation from experimental values increases.

The basic physical properties of the ordered $Cu_3Au(L1_2)$, $CuAu(L1_0)$ and $CuAu_3(L1_2)$ are listed in Table 4.8 with the experimental data whenever available [57, 69]. In this table, we also see that Q-SC potential predicts cohesive energy, lattice parameter, and density close to the experimental values than those of SC. In order to analyze the effects of temperature and concentration on the physical properties, these physical properties are presented in the same table up to 900 K. The increasing concentration of Au in Cu-Au compounds gives rise to decreasing cohesive energy of the Cu-Au intermetallics, while it causes an increment in lattice parameter and density, as expected.

4.4.1.2   Heat Capacity and volume thermal expansion

Specific heat can be determined from the differential of the enthalpy as follows;

Table 4.7: Comparisons of the lattice constant, cohesive energy, and density for Cu and Au pure metals, predicted from TPN ensemble at various temperatures using by Q-SC and SC potential parameters. First row corresponds to Q-SC calculation and second row refers to SC calculation at each temperature. The values in the parenthesis are the available experimental data [116].

Metals	T (K)	E_c (kJ/mole)	a (nm)	ρ (g/cm^3)
Cu(Fcc)	0	-339.566(-336.)	0.3593	9.097(9.018)
		-337.503	0.3616	8.930
	300	-331.765	0.3620(0.361)	8.899(8.9317)
		-329.912	0.3644	8.723
	400	-329.128	0.3629	8.829(8.8920)
		-327.267	0.3654	8.649
	500	-326.440	0.3639	8.757(8.8440)
		-324.553	0.3665	8.573
	600	-323.688	0.3649	8.683(8.800)
		-321.760	0.3676	8.494
	700	-320.845	0.3660	8.606(8.750)
		-318.880	0.3688	8.411
	800	-317.904	0.3672	8.526(8.7010)
		-315.884	0.3701	8.323
	900	-314.852	0.3684	8.441
		-312.759	0.3716	8.228
Au(Fcc)	0	-369.178(-368.)	0.4060(0.407)	19.548(19.488)
		-364.688	0.4078	19.285
	300	-361.596(-363.919)	0.4085(0.4080)	19.185(19.300)
		-357.042	0.4110	18.843
	400	-358.980	0.4095	19.056(19.219)
		-354.396	0.4122	18.684
	500	-356.320	0.4104	18.922(19.134)
		-351.694	0.4134	18.518
	600	-353.615	0.4114	18.784(19.043)
		-348.914	0.4147	18.344
	700	-350.850	0.4125	18.639(18.956)
		-346.045	0.4161	18.160
	800	-348.020	0.4136	18.488(18.866)
		-343.054	0.4176	17.960
	900	-345.093	0.4148	18.328
		-339.907	0.4193	17.742

Table 4.8: Comparisons of the lattice constant, cohesive energy, and density for ordered Cu-Au alloys, predicted from TPN ensemble at various temperatures. First row corresponds to Q-SC calculation and second row refers to SC calculation at each temperature. The values in the parenthesis are the experimental data whenever available [57, 69].

Metals	T (K)	E_c (kJ/mole)	a (nm)	c (nm)	ρ (g/cm^3)
Cu$_3$Au(L1$_2$)	0	-346.282(-350.441)	0.3727 (0.374)		12.427(12.331)
		-344.624	0.3746		12.240
	300	-338.624	0.3752		12.187(12.214)
		-336.925	0.3775		11.966
	373	-336.717	0.3758		12.125
		-335.006	0.3782		11.896
	473	-334.070	0.3767		12.038
		-332.330	0.3793		11.798
	573	-331.371	0.3777		11.948
		-329.581	0.3804		11.694
	673	-328.608	0.3787		11.854
		-326.750	0.3816		11.586
	723	-327.195	0.3792		11.806
		-325.291	0.3822		11.529
	800	-324.986	0.3800		11.730
		-322.995	0.3832		11.438
	900	-322.033	0.3811		11.626
		-319.881	0.3846		11.311
CuAu(L1$_0$)	0	-352.932(360.069)	0.3950(0.3966)	0.3659(0.3673)	15.148
	300	-346.277	0.3970(0.3966)	0.3678(0.3673)	14.9202
	400	-343.661	0.3980	0.3686	14.819
	500	-341.003	0.3989	0.3695	14.714
	600	-338.299	0.3999	0.3704	14.605
	700	-335.549	0.4009	0.3714	14.494
	800	-332.724	0.4020	0.3724	14.376
	900	-329.834	0.4031	0.3734	14.256

Table 4.9: Continued Table 4.8.

Metals	T	E_c	a	c	ρ
	(K)	(kJ/mole)	(nm)	(nm)	(g/cm^3)
CuAu$_3$(L1$_2$)	0	-360.919(-364.8822)	0.3965		17.429
		-357.405	0.3982		17.206
	300	-353.312	0.3990(0.398)		17.105
		-349.846	0.4012		16.822
	400	-350.709	0.3999		16.991
		-347.215	0.4023		16.685
	500	-348.064	0.4008		16.874
		-344.521	0.4035		16.541
	600	-345.365	0.4018		16.753
		-341.742	0.4047		16.390
	700	-342.615	0.4028		16.629
		-338.880	0.4061		16.230
	800	-339.799	0.4039		16.498
		-335.896	0.4075		16.058
	900	-336.886	0.4050		16.358
		-332.754	0.4091		15.870

$$C_p(T) = \left(\frac{\partial H(T)}{\partial T} \right)_p.$$ (4.17)

Coefficient of thermal volume expansion is calculated from the following;

$$\alpha_p(T) = -\frac{1}{V(T)} \left(\frac{\partial V(T)}{\partial T} \right)_p.$$ (4.18)

The enthalpy of Cu-Au alloys is fitted to a quadratic polynomial using the data below the melting temperature to analyze the heat capacity as a function of temperature and concentration. The quadratic function form may be chosen as;

$$H(T) = a + b\ T + c\ T^2 \quad kJ/mole \quad .$$ (4.19)

Here T is the temperature. Enthalpy values obtained between 300 K and 1000

Table 4.10: Coefficients of polynomial function used to find the heat capacity of Cu, Au pure metals and their alloys. Heat capacity values of the metals along with whenever available experimental data [141].

Metals	a	$b \times 10^{-4}$	$c \times 10^{-6}$	C_p (kJ mole^{-1} K^{-1}) This Work	C_p (kJmole^{-1} K^{-1}) Experiment
Cu	-338.967	227.341	4.530	0.025452	0.024464
Cu$_3$Au	-345.877	231.251	3.770	0.025387	
CuAu	-353.657	237.437	3.054	0.025576	
CuAu$_3$	-360.603	233.694	3.337	0.025371	
Au	-368.952	236.082	3.232	0.025548	0.025325

K are used in fitting. Heat capacity can be found by taking the derivative of the polynomial function of 4.19 according to Eq. (4.17). The resulting C_p should not be extrapolated to T=0 K, as it is derived from $H(T)$ which is fitted to simulation results between 300 K and 1000 K. The coefficients of expression of Eq. 4.19 are given in Table 4.4.1.2.

As shown in Table 4.4.1.2, agreement between the simulated results and experimental data given in Ref. [141] is very good. For example the heat capacities of Cu and Au are 0.024464 kJ mole^{-1} K^{-1} and 0.025325 kJ mole^{-1} K^{-1}, respectively. Deviations from the experimental values for Cu and Au are 4.03 % and 0.8 %, respectively.

We have also fitted the volume and temperature curve by the same type quadratic polynomial function as done in the heat capacity to analyze further the volume thermal expansion behavior. The function used in fitting procedure is given as;

Table 4.11: Coefficients of polynomial function used to find the thermal volume expansions of Cu, Au pure metals and their alloys. Thermal volume expansion values of the metals along with whenever available experimental data [141, 142].

Metals	$a \times 10^{-4}$	$b \times 10^{-9}$	$c \times 10^{-6}$	$\alpha_p \times 10^{-5}$ (K^{-1}) This Work	$\alpha_p \times 10^{-5}$ (K^{-1}) Experiment
Cu	116.019	757.735	268.129	7.750	4.95
Cu$_3$Au	129.496	750.845	290.589	7.009	
CuAu	142.443	748.488	316.017	6.471	
CuAu$_3$	155.908	867.780	293.112	6.573	4.77
Au	167.337	926.713	342.756	6.644	

$$V(T) = a + b \ T + c \ T^2 \quad nm^3/mole \qquad . \tag{4.20}$$

The coefficients for the expression of 4.20 and the values of the thermal volume expansion calculated from Eq. 4.18 at 300 K are presented in Table 4.4.1.2.

The value of copper, 7.750×10^{-05} K^{-1}, is in good agreement with the value from simulation calculation of Ref. [143]. But the calculated value is slightly greater than the experimental value, 4.95×10^{-05} [143].

4.4.2 Mechanical Properties

4.4.2.1 Elastic Constants and Bulk Modulus

The elastic constants of solids provide valuable information on mechanical and dynamical properties, in particular, they provide information on the stability and stiffness of materials. In this study, elastic constants are calculated by using the fluctuation expression 4.2 by taking the average ensemble of EVN over the 50000

time steps. The elastic constants and bulk modulus results for Cu and Au metals are listed in Table 4.12. At each temperature, density obtained from TPN ensemble by averaging over the 20000 time steps is used to specify the volume of the EVN ensemble. The detailed calculation methodology related to the elastic constants can be found in Refs. [111, 104]. The elastic constants and bulk modulus of Cu and Au pure metals predicted from Q-SC and SC parameters are compared with the available experimental values at four different temperatures in Table 4.12. The theoretical values of Cu for the Q-SC are less than experimental values at all given temperatures, whereas the situation is not the same the for SC calculations for Cu. The discrepancy between the calculated values and experimental values usually increases with the increasing temperatures above 300 K. The percentage differences of C_{11}, C_{12} and C_{44} of Cu for the Q-SC are 9.8 %, 2.9 % and 11.1 % at 0 K, respectively. In the case of SC calculation, these percentage differences are 2.3 %, 18.4 %, 48.5 % at 0 K, respectively. For the results of Q-SC of Au, they are 4.5 %, 3.9 % and 33.6 % at 0 K, whereas they are 24 %, 30 %, and 8.8 % for SC. The differences between the Q-SC and experimental values are generally less than SC results for both Cu and Au pure metals. This is not surprising since the Q-SC potential parameters were chosen to reproduce more experimental results.

The maximum deviations of bulk modulus of Cu and Au for Q-SC are 11 % and 8.9 % at 500 K, respectively, as shown in Table 4.12. On the other hand, the largest deviations of Cu and Au for SC are 11.70 % at 0 K and 24 % at 300 K,

Table 4.12: Elastic constants and bulk modulus of Cu and Au pure metals at various temperatures, calculated from EVN ensemble over the 50000 time steps. Elastic constants and bulk modulus are in units of GPa. Bulk moduli are calculated from the expression B=(C_{11}+2 C_{12})/3. First row corresponds to Q-SC calculation and second row refers to SC calculation. The values in the parenthesis are the available experimental data [120].

Metals	T(K)	C_{11}	C_{12}	C_{44}	B
Cu (Fcc)	0	158.996(176.20)	121.296(124.94)	72.736(81.8)	133.554(142.026)
		180.066	147.937	42.131	158.645
	300	154.272(168.4)	110.432(121.42)	63.256(75.39)	124.746(137.080)
		157.430	130.893	34.798	139.709
	400	148.659(165.50)	107.660(120.50)	60.354(73.10)	121.232(135.5)
	500	144.221(161.50)	105.139(118.50)	57.328(70.40)	118.174(132.830)
Au (Fcc)	0	210.617(201.6)	163.011(169.7)	60.660(45.4)	178.879(180.333)
		152.736	119.163	49.396	130.510
	300	188.844(192.3)	147.829(163.1)	51.892(41.95)	161.413(172.833)
		152.736	119.163	49.396	130.510
	400	183.614(189.00)	144.481(160.5)	48.960(41.00)	157.537(170.000)
	500	176.560(185.00)	140.213(158.00)	46.408(39.70)	152.065(167.000)

respectively.

We have also calculated the elastic constants and bulk modulus of Cu-Au ordered intermetallic alloys to see the temperature and concentration effects on the results. The simulation results for the Q-SC and SC potential parameters and available experimental data are listed in Table 4.13. In these elastic constants, the maximum deviations in C_{44} of Cu_3Au for SC calculations are 27 % at 0K, the largest deviation in C_{44} for $CuAu_3$ is 36.7 %. Other deviations are acceptable error range for both SC and Q-SC. Here, we also present the elastic constants of CuAu ordered metal alloy in structure of $L1_0$ for the case c/a=1. The simulations results are not compared with any experimental and theoretical data not present in the literature. The bulk modulus are also given in the same table with the experimental data whenever available.

In Table 4.14, the contributions of kinetic-energy, fluctuation, and Born terms to elastic constants for the Cu_3Au are tabulated separately to show the respective weights of these terms in the simulations results. As shown in Table 4.14, the largest contributions come from the Born terms to elastic constants. The fluctuation contributions are negative for all elastic constants except for C_{12} at 0 K. Fluctuation contributions increase as the temperature increases. This is due to a broader distribution of the microscopic stress tensor. The kinetic energy terms are small (1-2 %) for all elastic constants at various temperatures. But they increase as the temperature increases except for all C_{12}. The kinetic energy terms of all C_{12} are zero because of the existence of Kronecker delta in Eq. 4.2.

Table 4.13: Elastic constants and bulk modulus of $Cu_3Au(L1_2)$, $CuAu(L1_0)$ for the ratio of c/a=1.0 and $CuAu_3$ ordered intermetallic alloys at various temperatures, calculated from EVN ensemble. Elastic constants and bulk modulus are in units of GPa. Bulk modulus are calculated from the expression of $B=(C_{11}+2 C_{12})/3$ for the cubic systems. First row corresponds to Q-SC calculations and second row refers to SC calculations. The values in the parenthesis are the experimental data [120].

Metals	T(K)	C_{11}	C_{12}	C_{44}	B
$Cu_3Au(L1_2)$	0	180.616(189.30)	134.299(131.90)	71.480(73.60)	149.653
		175.347	135.863	53.723	149.032
	300	169.901(187.10)	123.631(134.90)	62.112(67.80)	139.228
		158.234	124.252	45.203	135.454
	373	166.225	121.473	59.933	136.103
	473	160.558	119.116	56.381	133.062
	573	153.857	115.497	53.051	128.261
	673	148.351	112.786	50.227	124.411
	723	145.804	111.540	48.795	122.895
	800	140.535	108.586	46.219	119.011
$CuAu((L1_0)$	0	210.427	149.906	72.576	205.586
	300	191.663	139.097	62.056	186.782
	400	184.303	135.399	59.168	179.881
	500	178.549	132.170	55.964	174.358
$CuAu_3(L1_2)$	0	206.946(189)	154.415(155)	64.267(47)	171.928(166)
		180.794	143.826	45.2840	156.148
	300	187.494	141.997	54.8626	156.846
		158.711	128.636	37.1720	138.514
	400	180.441	137.550	51.845	151.742
		152.600	124.456	34.795	133.867
	500	174.859	134.525	48.965	147.639
		145.303	120.067	32.137	128.788

Table 4.14: The contributions to elastic constants of Cu_3Au intermetallic alloy from Born, fluctuation, and kinetic energy terms for the Q-SC calculations. The units are in GPa.

T (K)		Born term	Fluctuation term	Kinetic energy term	Total
0	C_{11}	186.690	-6.074	0.000	180.616
	C_{12}	131.980	2.319	0.000	134.299
	C_{44}	71.483	-0.026	0.000	71.480
300	C_{11}	179.489	-10.85	1.262	169.901
	C_{12}	126.600	-2.969	0.000	123.631
	C_{44}	68.190	-6.709	0.631	62.112
473	C_{11}	174.754	-16.141	1.946	160.558
	C_{12}	123.086	-3.970	0.000	119.116
	C_{44}	65.962	-10.554	0.973	56.381
573	C_{11}	171.827	-20.290	2.319	153.857
	C_{12}	120.925	-5.428	0.000	115.497
	C_{44}	64.572	-5.480	1.160	50.227

4.4.3 Melting Temperature

Figure 4.25 presents the simulated lattice parameter a of ordered Cu_3Au alloy as a function of temperature, along with available experimental data [56]. There is obviously a discontinuity in the Fig. 4.25. This may be due to a phase trans-formation of the material. If the pair distribution function is examined around the melting region, the peaks after the second one disappear, and it is oscillatory 'around the 1. Other physical properties such as enthalpy, density, and diffusion are also considered in determining the melting point. Computer simulations are carried out by 10 K increments around the discontinuity to calculate the melt-ing points better. In this manner, the melting points of the pure elements and intermetallic systems are calculated for both Q-SC and SC parameter sets. The

87

Table 4.15: Melting points of Cu-Au ordered alloys and Cu and Au pure metals along with experimental [115] and other computational results [68].

Cu-Au alloys	$T_m^{cal.}$(K) Q-SC	$T_m^{cal.}$(K) SC	$T_m^{exp.}$(K)	Deviation (%) Q-SC	SC	T_m^{others}(K)
Cu(Fcc)	1370±10	1150±10	1356	1.03	15.19	1320.5±1.5
$Cu_3Au(L1_2)$	1340±10	1110±10	1250	7.20	11.20	1240.5±1.5
$CuAu(L1_0)$	1360±10		1185	14.76	-	1173.5±0.5
CuAu(Fcc)	1370±10			15.61	-	
$CuAu_3(L1_2)$	1370±10	1020±20	1220	12.30	16.39	1151.5±1.5
Au	1420±10	1120±10	1336	6.29	16.16	1182.5±1.5

results found for the melting points are listed in Table 4.15 along with the available experimental [115] and other theoretical data [68]. The deviations of melting points from experiments for Q-SC are less than SC calculations. This indicates that Q-SC potential produce more accurate results at higher temperatures. The melting point also indicate the validity of potential parameters. The melting point of CuAu is predicted for both structures of $CuAu(L1_0)$ and $CuAu(L1_0)$ having c/a=1. The melting point of $CuAu(L1_0)$ is closer to the experimental value. The deviations of SC calculation are greater than those of Q-SC. This is an indication of the transferability of the Q-SC parameters from low temperatures to high temperatures, and from elemental to intermetallic alloys. Next, this will be tested by calculating the liquid properties such as diffusion, viscosity, and structural properties of considered metals.

4.4.4 Phonon Frequency

As explained in Section 4.1.3, the phonon dispersion relations calculated from both Q-SC and SC parameters for the Cu, Au pure metals, ordered Cu_3Au and
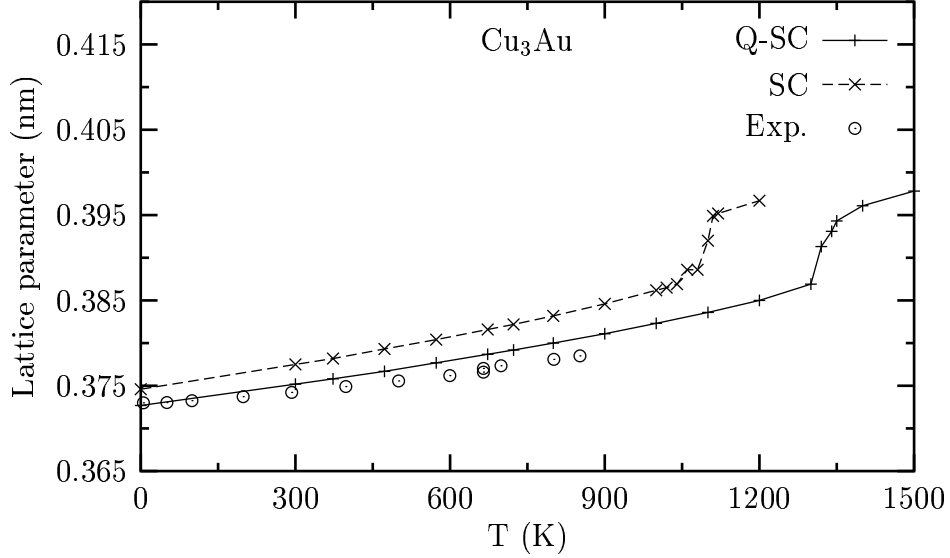
Figure 4.25: Lattice parameter of the Cu_3Au as a function of temperature for both Q-SC and SC, the circle points are experimental data from Ref. [56].

$CuAu_3$ intermetallic compounds are shown in Figs. 4.26, 4.27, 4.28, and 4.29, respectively. As shown in Figs. 4.26 and 4.29, the improvement in the Q-SC calculations over the SC results is clear. The same remark may be made on the phonon dispersion of the Cu_3Au. The overall structure of the phonon dispersion curves is well reproduced. The result for $CuAu_3$ is not compared with the any experimental or theoretical data; these are not available in the literature. It should be noted that the phonon spectra is calculated over the entire Brillouin zone while the fit in terms of phonon spectra was done only for the X point. We may have to note the fact that although original SC potential has been fitted only tree experimental quantities such as lattice parameter, cohesive energy, and bulk

89

Figure 4.26: Phonon dispersion curves of Cu at room temperature for Q-SC and SC potential parameters, the circles show experimental data from Ref. [144] at 300 K.

modulus, it gives compatible results at all points of phonon dispersion curves.

Figure 4.27: Phonon dispersion curves of Cu_3Au and at room temperature for Q-SC and SC potential parameters, the circles are experimental data from Ref. [145] at 300 K.

Figure 4.28: Phonon dispersion curves of $CuAu_3$ at room temperature for Q-SC and SC potential parameters.
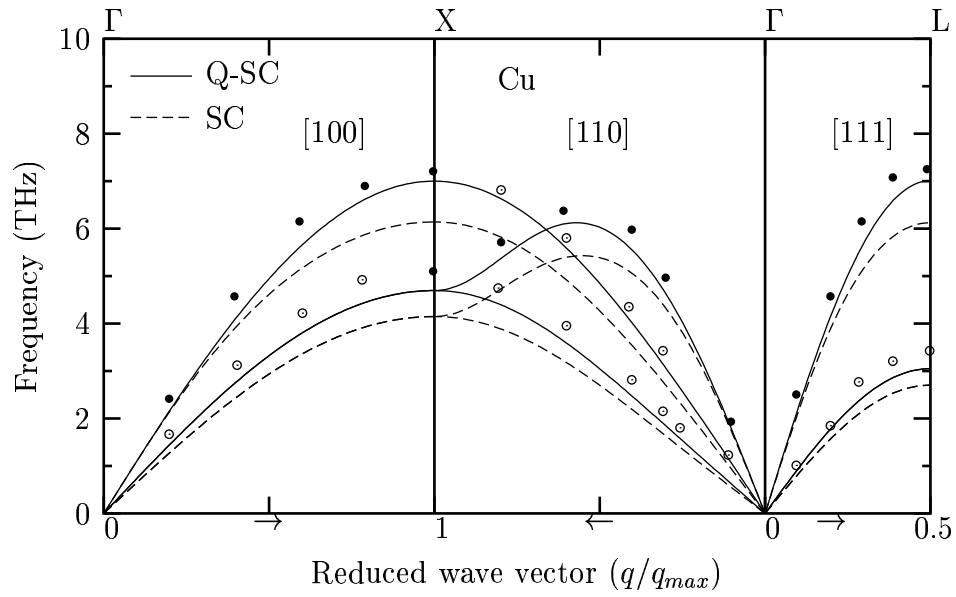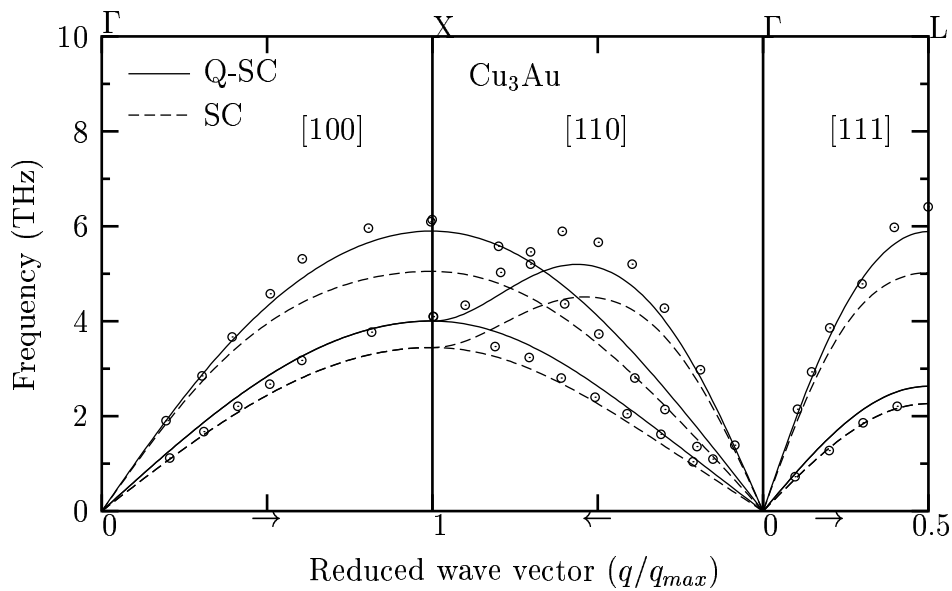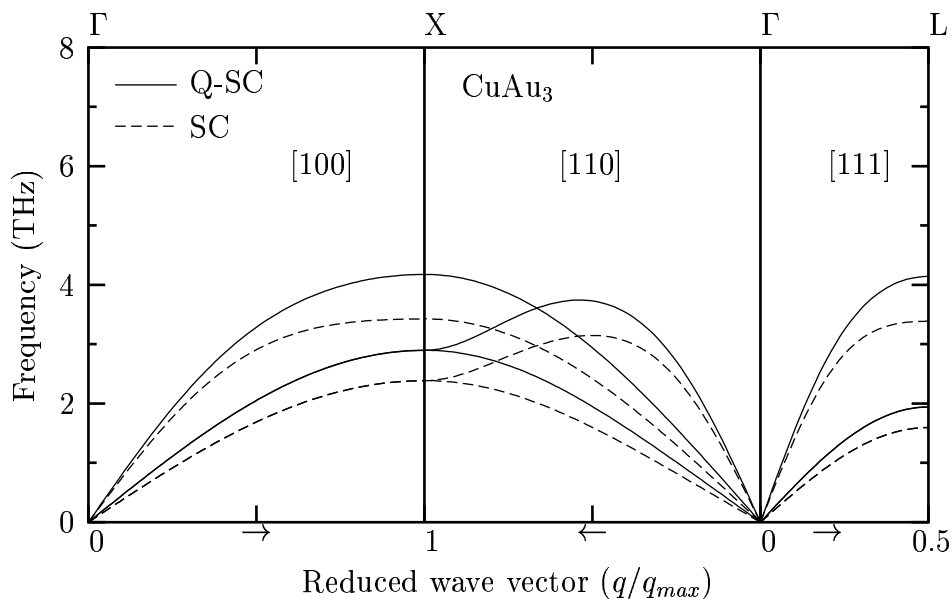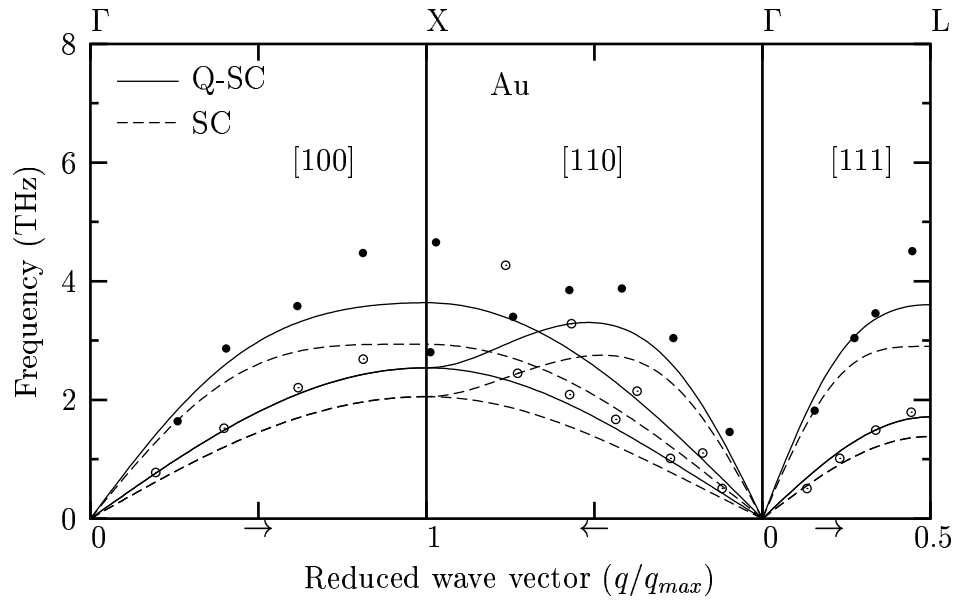
Figure 4.29: Phonon dispersion curves of Cu at room temperature for Q-SC and SC potential parameters, the circle points are experimental data from Ref. [144] at 300 K.

CHAPTER 5

CONCLUSION

We have investigated extensively mechanical, thermodynamical and melting properties of Pd, Ag metals and their binary alloys Pd_xAg_{1-x} using the Sutton-Chen and quantum Sutton-Chen potential parameters.

We have presented elastic and thermodynamical properties such as elastic constants (C_{11}, C_{12}, C_{44}), bulk modulus (B), lattice parameter (a), cohesive energy (E_c), and density (ρ) for the Pd-Ag alloys at different concentrations for the first time. The agreement between the estimated melting points and experimental values are acceptable for the pure and alloy case. As for comparison in the case of alloy, we have found experimental data for mechanical and thermodynamical properties of ($Pd_{0.0622}Ag_{0.9378}$) at room temperature only for one concentration. Simulation results at this concentration are in good agreement with the available experimental data. In addition to these calculations, transverse and longitudinal phonon modes are calculated in the [100], [110], and [111] directions. Our calculations for Pd are closer to the experimental data than EAM calculation performed by Daw and Hatcher [146]. It may be underlined that although the original SC potential parameters have been fitted to only three experimental quantities it still gives good agreement with the experimental data. Our calculated melting

points are closer to the experimental values than those calculated by others, as seen from Table 4.3. The Q-SC potential works better in predicting the melting temperatures for Pd-Ag system than the SC potential.

The results obtained are very helpful for a deeper understanding of the chosen materials and these results also provide a useful guide for the improvement of the potentials for real systems. We have shown that Q-SC potential parameters appear to be convenient for transferability from pure metals to binary alloys without further empirical fitting to properties of Pd_xAg_{1-x} with the combination rules. Q-SC potential parameters which are fitted to experimental properties such as density, cohesive energy, moduli, and phonon frequencies while including the zero-point energy effects generate useful information about the chosen pure and alloy systems except for elastic constants. It is concluded that the potential must be fitted to give solid properties of the alloy at the specific concentration correctly. This could improve the results further.

When the temperature increases, the local structure of the solid is lost and a diffusional dynamics becomes dominant, as seen from the pair distribution function and velocity auto-correlation functions. We have calculated diffusion coefficients which distinguish the liquid from the solid using both the Einstein relation and Green-Kubo formula. The diffusion coefficients obtained are in agreement with the experimental and theoretical values, as shown in Table 4.4. Especially, diffusion coefficient value of 2.77 (nm^2/ns) for Ag, which is obtained from Einstein relation in the TPN ensemble, is closer to experimental value of 2.81 (nm^2/ns)

at 1273 K [132]. The diffusions coefficients which are calculated by fitting to the Eq. 4.15 for Pd and Ag in the EVN are also mutually consistent with each other and agree very well with Alemany's diffusion coefficient values which are computed by using the second-moment approximation to the tight-binding method and the embedded atom model [133, 134]. The temperature dependence of the self-diffusion coefficient seems to be described well by the Arrhenius law. The concentration effects on the diffusion and viscosity for Pd-Ag alloys show that the values of self-diffusion of Pd-Ag alloys increase while viscosity values of the alloys decreases as expected by increasing the concentration of Ag in Pd. The Arrhenius fitting parameters are presented in this study to predict the self-diffusion and shear viscosity values of Pd-Ag alloys. Transferability of SC and Q-SC potential parameter sets from solid to liquid metal phases are tested by examining the structural and dynamical properties of the metals considered here. The results of the present work show that this could be done better with the Q-SC parameter set. We emphasize that if the SC potential is fitted to the pure and alloy liquid experimental properties, the results may be improved further.

The glass formation and crystallization of binary $Pd_x Ag_{1-x}$ alloys are also studied by using the Q-SC potential. We have obtained a wide range of valuable physical properties of $Pd_x Ag_{1-x}$ in the liquid, crystal, and glass phases. Glass transition is not a first-order transition, as shown in Fig.4.19. Indeed there is not a unique glass state since its properties depend on how it is achieved. We

95

have observed that as the simulation time of the system increases the corresponding crystallization temperature increases. A long simulation time is necessary to crystallize the model system with increasing concentration of Ag in the Pd-Ag alloy. The self-diffusion coefficients are calculated to compare their behavior during both heating and cooling processes. It is seen that Pd-Ag forms a metallic glass at fast cooling rates and it crystallizes at slow cooling rates. The glass transition and crystallization temperatures depend on the chosen cooling rates. The results are very helpful for a deeper understanding of the basis of the behavior of liquid, crystal, and glass formation tendency. This study shows that the Q-SC potential is practical for studying the crystallization and glass formation properties of transition metals and their alloys. It would be interesting to test the predictions of the present work with the results of a first-principle simulation study, in the absence of specific experimental data for Pd-Ag alloys.

We have also presented wide range of properties of Cu, Au pure metals and their Cu_3Au, $CuAu$, and $CuAu_3$ ordered intermetallics. Q-SC potential parameters provide fairly accurate temperature dependent properties of both pure elements and ordered systems studied here at low and high temperatures. The results demonstrate the transferability of the Q-SC parameters from low to high temperatures and from elemental to intermetallic alloys. The reason for improvement of Q-SC over SC may be due to the parametrization followed in the procedure followed in Q-SC. If the potential energy function considered here is fitted to the solid properties of the intermetallic compounds of Cu_3Au, $CuAu$,

and $CuAu_3$ the results may be improved further.

The intermetallic results obtained here lead us to believe that Q-SC potential may produce accurate results of the liquid and glass properties of Cu_3Au, $CuAu$, and $CuAu_3$. This should be checked separately.

To sum up, finding the minimum energy configuration of atoms in the simulation box by using the Monte Carlo simulation may improve the MD results further. A better improvement in the results may be obtained by including the electrons to the ionic system and by performing a first-principle MD, which gives excellent results for systems that can be described by a relatively small number of atoms.

REFERENCES

[1] H. Rafii-Tabar, Phys. Rep. **390**, 235-452 (2004).

[2] H. Rafii-Tabar and A. Chirazi, Phys. Rep. **365**, 145-249 (2002).

[3] H. Rafii-Tabar, Phys. Rep. **325**, 239-310 (2000).

[4] N. M. Ghoniem, E. P. Busso, N. Kioussis, and H. Huang, Phil. Mag. **83**, 3475-3528 (2003).

[5] D. G. Papageongiou, I. E. Lagaris, N. I. Papanicolaou, G. Petsos, and H. M. Polatoglou, Comp. Mat. Sci. **28**, 125-133 (2003).

[6] A. A. Selezenev, A. Y. Aleynikov, N. S. Gantchuk, P. V. Yermakov, J. K. Labanowski, and A. A. Korkin, Comp. Mat. Sci. **28**, 107-124 (2003).

[7] K. Ohno, K. Esfarjani, and Y. Kawazoe, *Computational Material Science*, Springer-Verlag, Berlin (1999), p:283.

[8] N. W. Ashcroft and N. D. Mermin, *Solid State Physics*, saunders College, Orlando (1976), p:208.

[9] R. Car and M. Parrinello, Phys. Rev. Lett. **55**, 2471 (1985).

[10] Ş. Erkoç, Phys. Rep. **278**, 79-105 (1997).

[11] M. Finnis, Prog. in Mat. Sci. **49**, 1-18 (2004).

[12] M. S. Daw and M. I. Baskes, Phys. Rev. B **29**, 6443-6453 (1984).

[13] M. W. Finnis and J. E. Sinclair, Phil. Mag. A **50**, 45-55 (1984).

[14] F. Ercolassi, M. Parrinello, and E. Tosatti, Phil. Mag. A **58**, 213 (1988).

[15] A. P. Sutton and J. Chen, Phil. Mag. Lett. **61**, 139-146 (1990).

[16] M. Verstraete, J. Dumont, F. Mirabella, F. Wiame, K. Temst, J. Swerts, J. Ghijsen, R. Sporken, and X. Gonze, Comp. Mat. Sci. **30**, 34-43 (2004).

[17] J. K. Nórskov, Phys. Rev. B **26**, 2875-2885 (1984).

[18] N. I. Papanicolaou, G. C. Kallinteris, G. A. Evangelakis, D. A. Papaconstantopoulos, and M. J. Mehl, J. Phys.:Condens. Matter **10**, 10979 (1998).

[19] N. I. Papanicolaou and D. A. Papaconstantopoulou, Thin Solid Films **428**, 40-46 (2003).

[20] H. Feraoun, H. Aourag, T. Grosdidier, D. Klein, and C. Coddet, Superlatt. Microstruct. **30**, 261 (2001).

[21] H. Feraoun, C. Esling, L. Dembinski, T. Grosdidier, C. Coddet, and H. Aourag, Superlatt. Microstruct. **31**, 297 (2002).

[22] O. M. Lovvik and R. A. Olsen, J. All. Comp. **330-332**, 332-337 (2002).

[23] H. B. Liu, Z. Q. Hu, and G. Y. An, Phil. Mag. B **79**, 981-991 (1999).

[24] J. -F. Wax, N. Jakse, and I. Charpentier, Physica B **337**, 154-164 (2003).

[25] Y. Qi, T. Çağın, Y. Kimura and W. A. Goddard III, J. Comp. Aid. Mat. Des. **8**, 233-243 (2002).

[26] M. Asta, D. Morgan, J. J. Hoyt, B. Sadigh, and S. M. Foiles, Phys. Rev. B **59**, 14271-14281 (1999).

[27] M. Ji and X. G. Gong, J. Phys.:Condens. Matter **16**, 2507-2514 (2004).

[28] A. S. Chauhan, R. Ravi, and R. P. Chhabra, Chem. Phys. **252**, 227 (2000).

[29] H. I. Guntherodt and H. Beck, *Glassy Metals I*, Springer, New York (1981).

[30] H. I. Guntherodt and H. Beck, *Glassy Metals III*, Springer-Verlag, Heidelberg (1994).

[31] W. Götze and L. Sjögren, Rep. Prog. Phys. **55**, 241 (1992).

[32] A. Hunt, J. Non-Cryst. Solids **160**, 241 (1993).

[33] S. N. Nagel and J. Tauc, Phys. Rev. Lett. **35**, 380 (1987).

[34] J. Hafner, Phys. Rev. B **21**, 406 (1980).

[35] H. Choiyim and W. L. Johnson, Appl. Phys. Lett. **71**, 3808 (1997).

[36] R. Buch, JOM **52** (7), 39 (2000).

[37] M. D. Ediger, C. A. Angell and, S. R. N., J. Phys. Chem. **100**, 13200 (1996).

[38] F. Faupel, W. Frank, M. P. Macht, H. Mehrer, V. Naundorf, K. Rätzke, H. R. Schober, S. K. Sharma, and H. Teichler, Rev. Mod. Phys. **74**, 237 (2003).

[39] S. Schneider, J. Phys.: Condens. Matter **13**, 7723 (2001).

[40] J. F. Löffler, Intermetallics **11**, 529 (2003).

[41] T. Egami, J. Non-Cryst. Solids **317**, 30 (2003).

[42] W. Kob, J. Phys.: Condens. Matter **11**, R85 (1999).

[43] C. Hausleitner, M. Tegze, and J. Hafner, J. Phys.:Condens. Matter **4**, 9557 (1992).

[44] A. Peker and W. L. Johnson, Appl. Phys. Lett. **63**, 2342 (1993).

[45] X. H. Liu and W. L. Johnson, J. Appl. Phys. **78**, 6514 (1995).

[46] L. Hui, B. Xiufang, and W. Guanghou, Mat. Sci. and Eng. A **298**, 245-250 (2001).

[47] L. Wang, X. Liu, Y. Zhang, H. Yang, Y. Chen, and X. Bian, Phys. Lett. A **319**, 518-522 (2003).

[48] W. Klement, R. Wilens, and P. Duwez, Nature **187**, 869 (1960).

[49] N. S. Stoloff, C. T. Liu, and S. C. Deevi, Intermetallics **8**, 1313-1320 (2000).

[50] C. T. Liu, J. Stringer, J. N. Mundy, L. L. Horton and P. Angelini, Intermetallics **5**, 579-596 (1997).

[51] R. W. Cahn, Comtemporary Physics **42**, 365-375 (2001).

[52] N. I. Papanicolaou, H. Chamati, G. A. Evangelakis, and D. A. Papaconstantopoulos, Comp. Mat. Science **27**, 191-198 (2003).

[53] Y. Wang, Z. -K. Liu, L.-Q. Chen, Acta Materialia **52**, 2665-2671 (2004).

[54] Y. Mishin, M. J. Mehl and D. A. Papaconstantopoulos, Phys. Rev. B **65**, 224114 (2002).

[55] H. B. Liu, Z. Q. Hu, and G. Y. An, Phill. Mag. B **79** (7), 981-991 (1999).

[56] G. D. Barrera, R. H. de Tendler, Comp. Phys. Com. **105**, 159-168 (1997).

[57] S. -H. Wei, A. A. Mbaye, L. G. Ferreira, and A. Zunger, Phys. Rev. B **36**, 4163 (1987).

[58] D. G. Papageorgiou, I. E. Lagaris, N. I. Papanicolaou, G. Petsos, and H. M. Polatoglou, Comp. Mat. Sci. **28**, 125-133 (2003).

[59] L. Wang, Y. Zhang, H. Yang, and Y. Chen, Phys. Lett. A **317**, 489-494 (2003).

[60] V. Ozalins, C. Wolverton, and Alex Zunger, Phys. Rev. B **57**, 6427 (1998).

[61] G. J. Ackland and V. Vitek, Phys. Rev. B **41**, 10324 (1990).

[62] F. Cleri and V. Rosato, Phys. Rev. B **48**, 22 (1993).

[63] N. I. Papanicolaou, G. C. Kallinteris, G. A. Evangelakis, D. A. Papaconstantopoulos, and M. J. Mehl, J. Phys.: Condens. Matter **10**, 10979 (1998).

[64] S. Katano, M. Lizumi, and Y. Noda, J. Phys. F: Met. Phys. **18**, 2195-2202 (1988).

[65] P. Weinberger, V. Drchal, L. Szunyogh, and J. Fritscher, Phys. Rev. B **49**, 13366 (1994).

[66] J. W. Davenport, R. E. Watson, and M. Weinert, Phys. Rev. B **37**, 9985 (1988).

[67] J. Kudrnosky, S. K. Bose, O. K. Andersen, Phys. Rev. B **43**, 4613 (1991).

[68] X. J. Han, M. Chen, and Z. Y. Guo, J. Phys.:Condens. Matter **16**, 705-713 (2004).

[69] G. D. Barrera, R. H. de Tendler, and E. P. Isoardi, Modelling Simul. Mater. Sci. Eng. **8**, 389-401 (2000).

[70] J. Cai and Y. Y. Ye, Phys. Rev. B **54**, 8398 (1996).

[71] A. V. Ruban, I. A. Abrikosov, and H. L. Skriver, Phys. Rev. B **51**, 12958 (1995).

[72] N. Metadjer, A. Laref, B. Khelifa, C. Mathieu, S. Bresson, and H. Aourag, Superlattice and Microstructures **30**, 21-28 (2001).

[73] J. M. Haile, *Molecular Dynamics Simulation*, Wiley & Sons Publication, Canada (1992).

[74] T. Çağın, Y. Qi, H. Li, Y. Kimura, H. Ikeda, W. L. Jonhson, and W. A. Goddard III, MRS Symp. Ser. **554**, 43-48 (1999).

[75] M. P. Allen and D. J. Tildesley, *Computer Simulation of Liquids*, Oxford Science Publications, New York (1987).

[76] D. C. Rapaport, *The Art of Molecular Dynamics Simulation*, Cambridge University Press, Cambridge (1995).

[77] D. W. Heermann, *Computer Simulation Methods*, Springer-Verlag, Berlin (1990).

[78] D. C. Young, *Computational Chemistry; A Practical Guide for Applying Techniques to Real-World-Problems*, John Wiley-Sons, (2001) p:60.

[79] B. J. Alder and T. E. Wainwright, J. Chem. Phys. **27**, 1208 (1957).

[80] B. J. Alder and T. E. Wainwright, J. Chem. Phys. **31**, 459 (1959).

[81] A. Rahman, Phys. Rev. Lett. **136**, A405 (1964).

[82] A. Rahman, Phys. Rev. Lett. **12**, 575 (1964).

[83] A. Rahman, J. Chem. Phys. **45**, 258 (1966).

[84] L. Verlet, Phys. Rev. **159**, 98 (1967).

[85] L. Verlet, Phys. Rev. **163**, 201 (1968).

[86] D. Levesque and L. Verlet, Phys. Rev. A **2**, 2514 (1970).

[87] D. Levesque, L. Verlet, and J. Kürkijarvi, Phys. Rev. A**7**, 1690 (1973).

[88] H. C. Andersen, J. Chem. Phys. **72**, 2384 (1980).

[89] S. Nosé, Mol. Phys. **52**, 255 (1984).

[90] S. Nosé, J. Chem. Phys. **81**, 511 (1984).

[91] M. Parrinello and A. Rahman, Phys. Rev. Lett. **45**, 1196 (1980).

[92] M. Parrinello and A. Rahman, J. Appl. Phys. **52**, 7182 (1981).

[93] W. G. Hoover, Phys. Rev. A **31**, 1695 (1985).

[94] T. Çağın and B. M. Pettitt Mol. Phys. **72**, 169 (1991); Mol. Sim. **6**, 5 (1991).

[95] D. Frenkel and B. Smit, *Understanding Molecular Simulation from Algorithms to Applications*, Academic Press, San Diego (1996).

[96] A. R. Leach, *Molecular Modelling Principles and Applications*, Longman, Edinburg (1997).

[97] C. W. Gear, *Numerical Initial Value Problems in Ordinary Differanstial Equations*, Prentice-Hall, NJ (1971).

[98] D. P. Tieleman and H. J. C. Berendsen, Biophys. J. **74**, 2786 (1998).

[99] M. S. Daw and M. I. Baskes, Phys. Rev. Lett. **50**, 1285 (1984).

[100] M. S. Daw, S. M. Foiles, and M. I. Baskes, Mat. Sci. Rep. **9**, 251-310 (1993).

[101] F. Ercolassi, E. Tosatti and M. Parrinello, Phys. Rev. Lett. **57**, 719 (1986).

[102] H. Rafii-Tabar and A. P. Sutton, Phil. Mag. Lett. **63**, 217 (1991).

[103] T. Çağın, G. Dereli, M. Uludoğan, and M. Tomak. Phys. Rev. B **59**, 3468-3472 (1999).

[104] G. Dereli, T. Çağın, M. Uludoğan, and M. Tomak, Phil. Mag. Lett. **75**, 209 (1997).

[105] Y. Qi, T. Çağın, Y. Kimura, and W. A. Goddard III, Phys. Rev. B **59**, 3527-3533 (1999).

[106] H. J. Lee, T. Çağın, W. L. Johnson, and W. A. Goddard III, J. Chem. Phys. **119**, 9858 (2003).

[107] Y. Qi, T. Çağın, W. L. Johnson, and W. A. Goddard III, J. Chem. Phys. **115**, 385 (2001).

[108] A. Strachan, T. Çağın, and W. A. Goddard III, Phys. Rev. B **63**, 0601103 (2001).

[109] H. Ikeda, Y. Qi, T. Çağın, K. Samwer, W. L. Jonhson, and W. A. Goddard III, Phys. Rev. Lett. **82**, 2900 (1999).

[110] H. H. Kart, M. Uludoğan, T. Çağın, and M. Tomak, *Simulation of crystallization and glass formation processes for binary Pd-Ag metal alloys*, Nanoenginered Nanofibrous Materials, Nato Science Series by S. Güceri, Y. Gogotsi and W. Kuzentsov, Kluwer Academic Book Publishers, Netherlands (2004).

[111] H. H. Kart, M. Tomak, M. Uludoğan and T. Çağın, *Thermodynamical and mechanical properties of Pd-Ag alloys*, Comp. Mat. Sci. (2004), in press.

[112] H. H. Kart, M. Tomak, M. Uludoğan, and T. Çağın, *Structural and dynamical properties of liquid Pd-Ag alloys*, Int. J. Mod. Phys. B (2004), in press.

[113] H. H. Kart, M. Uludoğan, T. Çağın, and M. Tomak, *Simulation of crystallization and glass formation of binary Pd-Ag metal alloys*, J. Non-Crys. Solids **342**, 6-11, (2004).

[114] S. Özdemir Kart, M. Tomak, M. Uludoğan, and T. Çağın, J. Non-Cryst. Solids **337**, 101 (2004).

[115] R. Hultgren, D. D. Desai, and D. T. Hawkins, *Selected Values of Thermodynamic Properties of Binary Alloys*, Metal Park OH: ASM (1973).

[116] C. Kittel, *Introduction to Solid State Physics*, Wiley, New York (1996).

[117] F. Cleri and V. Rasato, Phys. Rev. B **48**, 22 (1993).

[118] T. Çağın and R. Ray, Phys. Rev. B **38**, 7940-7946 (1988); Phys. Rev. B **37**, 699-705 (1988).

[119] W. Harrison, *Elementary Electronic Structure*, World Scientific (1999).

[120] G. Simmons and H. Wang, *Single Crystal Elastic Constants and Calculated Aggregate Properties*, MIT Press, Cambridge (1991).

[121] G. P. Srivastava, *The Physics of Phonons*, Adam Hilger (1990).

[122] A. A. Maradudin, E. W. Montroll, and G. H. Weiss, *Theory of Lattice Dynamics in the Harmonic Approximation*, Academic Press (1963).

[123] W. Cochran and F. R. S., *The Dynamic of Atoms in Crystals*, (1973).

[124] M. T. Dove, *Introduction to Lattice Dynamics*, Cambridge University Press, New York (1993).

[125] W. A. Kamitakahara and B. N. Brockhouse, Phys. Lett. **29 A**, 639 (1969).

[126] D. H. Dutton, B. N. Brockhouse, and A. P. Miller, Can. J. Phys. **50**, 2915 (1972).

[127] J. M. Holender, Phys. Rev. B **41**, 8054-8061 (1980).

[128] L. Gómez, A. Dobry and H. T. Diep, Phys. Rev. B **55**, 6265-6271 (1997).

[129] J. M. Foiles and J. B. Adams, Phys. Rev. B **40**, 5909 (1989).

[130] T. Iida and R. I. L. Guthrie, *The Physical Properties of Liquid Metals*, Clarendon Press, Oxford (1988).

[131] Y. Waseda, *The Structure of Non-Crystalline Materials*, Mc Graw-Hill, New York (1980).

[132] M. Shimoji and T. Itami, *Atomic Transport in Liquid Metals*, Tarns Tech Publication, Switzerland (1986).

[133] M. M. G. Alemany, C. Rey, and L. J. Gallego, J. Chem. Phys. **109**, 5175 (1998).

[134] M. M. G. Alemany, O. Dieguez, C. Rey, and L. J. Gallego, Phys. Rev. B **60**, 9208 (1999).

[135] J. Mei and J. W. Davenport, Phys. Rev. B **42**, 9682 (1990).

[136] I. Egry, G. Lohöfer, and S. Sauerland, J. Non-Cryst. Solids **830**, 156-158 (1993).

[137] I. Yokoyama, Physica B **271**, 230-234 (1999).

[138] L. Wang, X. Bian, and J. Zhang, J. Phys. B: At. Mol. Opt. Phys. **35**, 3575-3582 (2002).

[139] H. Li, F. Ding, G. Wang, J. Zhang, and X. Bian, Sol. Stat. Comm. **120**, 41-46 (2001).

[140] H. R. Wendt and F. F. Abraham, Phys. Rev. Lett. **41**, 1244 (1978).

[141] I. Barin, Thermochemical Data of Pure Substances, VCH, Verlegsgesellschaft mbH, D-6940 Weinheim, Federal Republic of Germany (1989).

[142] H. Mei Jin and P. Wu J. Alloys and Comp. **343**, 71-76 (2002).

[143] H. E. Alper and P. Politzer, J. Mol. Struc. (Theochem) **487**, 117-125 (1999).

[144] N. Singh, N. S. Banger, and S. P. Singh, Phys. Rev. B **38**, 7415 (1988).

[145] S. Katano, M. Lizumi, and Y. Noda, J. Phys. F: Met. Phys. **18**, 2195-2202 (1988).

[146] M. S. Daw and R. D. Hatcher, Sol. Stat. Comm. **56**, 697-699 (1985).

VITA

Hasan Hüseyin Kart was born in Akhisar-Manisa on March 1, 1972. After having graduated from İzmir Motor Technical High School in 1989, he joined to the Physics Education Department of Dokuz Eylül University as a B.S. student. After receiving his B. Sc. degree in 1993, he received M.S. degree from the Department of Physics of Celal Bayar University. He succeeded in qualifying exam in May 2000 in the Physics Department at METU, Ankara. Presently, he works as a research assistant in the same department. He got married in September 2000 to Miss Sevgi Özdemir. He has a daughter.